The anti-sigma factor RsrA responds to oxidative stress by reburying its hydrophobic core

Karthik V. Rajasekar[1], Konrad Zdanowski[2,5], Jun Yan[3], Jonathan T. S. Hopper[3], Marie-Louise R. Francis[1], Colin Seepersad[1], Connor Sharp[1], Ludovic Pecqueur[4,6], Jörn M. Werner[4], Carol V. Robinson[3], Shabaz Mohammed,[1,3,] Jennifer R. Potts[2] & Colin Kleanthous[1]

[1] Department of Biochemistry, University of Oxford, South Parks Road, Oxford OX1 3QU, UK

[2] Department of Biology, University of York, York YO10 5DD, UK

[3] Chemistry Research Laboratory, University of Oxford, 12 Mansfield Road, Oxford OX1 3TA, UK

[4] School of Biological Sciences, University of Southampton, Bassett Crescent East, Southampton, SO16 7PX, UK

[5] Current address – Institute of Chemistry, University of Natural Sciences and Humanities, 3 Maja 54, 08-110 Siedlce, and Institute of Biochemistry and Biophysics Polish Academy of Sciences, Pawinskiego 5A, 02-106 Warsaw, Poland

[6] Current address – Chemistry of Biological Processes, Collège de France, 11 place Marcelin Berthelot, 75231 Paris Cedex 5, France.

Address for Correspondence: Prof Colin Kleanthous

Department of Biochemistry

University of Oxford

South Parks Road

Oxford OX1 3QU

UK

Tel: +44-1865-613370

Fax: +44-1865-613213

Email: colin.kleanthous@bioch.ox.ac.uk

Abstract

Redox regulated effector systems that counteract oxidative stress are essential for all forms of life. Here, we uncover a new paradigm for sensing oxidative stress centred on the hydrophobic core of a sensor protein. RsrA is an archetypal zinc-binding anti-sigma factor that responds to disulfide stress in the cytoplasm of Actinobacteria. We show that RsrA utilizes its hydrophobic core to bind the sigma factor σ^R preventing its association with RNA polymerase, and that zinc plays a central role in maintaining this high-affinity complex. Oxidation of RsrA is limited by the rate of zinc release, which weakens the RsrA-σ^R complex by accelerating its dissociation. The subsequent trigger disulfide, formed between specific combinations of RsrA's three zinc-binding cysteines, precipitates structural collapse to a compact state where all σ^R-binding residues are sequestered back into its hydrophobic core, releasing σ^R to activate transcription of anti-oxidant genes.

Introduction

All organisms must contend with the toxic effects of Reactive Oxygen Species (ROS), which include superoxide anion (O_2^-), hydrogen peroxide (H_2O_2) and the hydroxyl radical (OH•)[1,2], that covalently damage proteins, lipids and DNA[3]. ROS are by-products of aerobic metabolism which in mammals are implicated in the ageing process and diseases such as type 2 diabetes[4]. To minimise the build-up of disulfide bonds, one of the toxic consequences of ROS, organisms maintain a reducing cytoplasm through the production of millimolar concentrations of small molecule reducing agents such as glutathione[5]. A second line of defence is comprised of detoxification enzymes that decompose ROS, and the glutaredoxin/thioredoxin system of redox proteins that reduce cytoplasmic disulfide bonds[6]. Oxidative stress sensor proteins that lead to the activation of anti-oxidant genes form a third line of defence for maintaining redox homeostasis[7]. Sensor proteins are typically transcription factors or transcription factor inhibitors that contain reactive cysteines or metal centres which are directly modified by ROS[8,9]. Here, we focus on the disulfide stress sensor protein RsrA from *Streptomyces coelicolor*, which, in its resting state, blocks binding of the sigma factor σ^R to RNA polymerase (**Figure 1**)[10,11]. RsrA is a zinc-binding anti-sigma factor (ZAS) protein, the prototypical member of a large family of inhibitors of extracytoplasmic function (ECF) sigma factors that regulate bacterial responses to diverse stresses[12]. As yet, no molecular mechanism has been described for the stress-induced inactivation of any ZAS protein. We detail the mechanism by which RsrA responds to oxidation, releasing σ^R to mount the cellular antioxidant response.

ZAS proteins were originally identified by their $His_{xxx}Cys_{xx}Cys$ sequence motifs[11]. They share <30% sequence identity but are readily identified in bacterial genomes by their genomic location, downstream of an ECF (group IV) sigma factor[13]. ZAS proteins are further sub-divided by the identity of the fourth zinc coordination site, which is either a cysteine or histidine residue 23-26 amino acids N-terminal to the $His_{xxx}Cys_{xx}Cys$ motif (hereafter these two types of ZAS motifs are denoted as CHCC or HHCC, respectively), and if they contain

an additional domain or transmembrane region. RsrA is a soluble, single domain, CHCC-type ZAS motif protein while its paralogue ChrR[14] from the photosynthetic bacterium *Rhodobacter sphaeroides* is a HHCC-type ZAS motif protein, which has an additional cupin-like domain.

ZAS proteins respond to different stimuli, inducing them to release their cognate sigma factor to activate regulons that respond to the stress[12,15]. Homologues of the RsrA-σ^R complex are found throughout the actinomycetes, including *Mycobacterium tuberculosis* where the system has been shown to be important for pathogenesis[16], and *Corynebacterium diphtheriae*. In the case of *S. coelicolor*, σ^R is a global transcriptional regulator, activating a regulon of >100 genes that includes anti-oxidant genes (**Figure 1**)[17]. ChrR by contrast senses singlet oxygen stress, a toxic ROS by-product of photosynthesis[18,19]. Release of its sigma factor, σ^E (also known as RpoE), results in the increased production of carotinoids that quench the singlet oxygen radical[20]. RsiW from *Bacillus subtilis* is a membrane-bound ZAS protein that is proteolytically-degraded following cell envelope stress through the action of antibiotics such as vancomycin, releasing its ECF sigma factor to activate a regulon for detoxification of and protection against antimicrobials[21]. Structures for two ZAS proteins bound to their cognate ECF sigma factors have been reported, the intact ChrR-σ^E complex[13] and the isolated ZAS domain of RslA from *M. tuberculosis* bound to one of the two domains of σ^L [ref.22]. No structure has yet been reported for any ZAS protein in the absence of its sigma factor or in an inactivated state following stress-induced dissociation.

RsrA is a 105 amino acid protein that contains seven cysteines. Three of the cysteines, Cys11, Cys41 and Cys44, contribute to the CHCC ZAS motif and are essential for redox sensing *in vivo* and *in vitro*[23]. Zdanowski et al (2006) showed using EXAFS spectroscopy that all three cysteines, along with His37, also within the ZAS motif, coordinate a single zinc ion in both RsrA and the RsrA-σ^R complex[24]. Oxidation of RsrA is known to result in the loss of zinc and formation of a degenerate trigger disulfide bond, formed between Cys11 and either of Cys41 or Cys44 which blocks σ^R binding[25,26]. However, the

involvement of the metal ion in redox sensing remains enigmatic. Here we uncover this role and its structural basis. As well as revealing a new mechanism by which an oxidative stress sensor protein responds to changes in cellular redox status this study also lays the foundations for understanding how ZAS proteins function as generic stress sensors.

Results

We first re-assessed the stoichiometry of zinc binding to the wild type protein and a mutant in which the four non-essential cysteines (Cys3, Cys31, Cys61 and Cys62) were mutated to alanine (RsrA*). See Materials and Methods for details. Although multiple zinc ions can bind to reduced RsrA and RsrA* only a single zinc stabilises the protein fold (**Supplementary Figure 1**) and, as detailed below, modulates redox activity. We refer to this form as $RsrA^{red}.Zn^{2+}$.

Redox potential of $RsrA^{red}.Zn^{2+}$

A key question for an oxidative stress sensor is its redox potential as this will govern its reactivity towards oxidants. No such measurements have been reported for any ZAS protein. We therefore determined the redox potential for $RsrA^{red}.Zn^{2+}$ in complex with σ^R with reference to a glutathione redox couple. The status of the complex in these experiments was monitored by tryptophan emission fluorescence spectroscopy, where we exploited a significant change in σ^R fluorescence that occurs on forming its complex with $RsrA^{red}.Zn^{2+}$ (**Figure 2a**). The oxidation status of $RsrA^{red}.Zn^{2+}$ was determined spectrophotometrically by the stoichiometric release of zinc using 4-(2-pyridylazo) resorcinol (PAR; see Materials and Methods). The two datasets were in excellent agreement (**Figure 2b**) and showed the redox potential for $RsrA^{red}$-Zn^{2+} in complex with σ^R to be -193.04 ± 2.01 mV. Our data show that the redox potential of $RsrA^{red}.Zn^{2+}$ is ideally poised to act as a redox sensor. Its redox potential is close to that estimated for the bacterial cytoplasm (**Figure 2c**)[27], rendering it sensitive to small changes in the redox status of the cell.

Role of zinc in modulating σ^R binding and oxidation of RsrA

Using isothermal titration calorimetry (ITC) we determined that $RsrA^{red}.Zn^{2+}$ binds σ^R with sub-nanomolar affinity (**Figure 3a**), whereas RsrA devoid of zinc bound σ^R 100-fold more weakly (**Figure 3b**). Zinc-associated RsrA* bound σ^R with a similar affinity to wild type RsrA, while mutation of any zinc-binding cysteine residue decreased σ^R binding by >100-fold (**Supplementary Table 1**). We conclude that the $RsrA^{red}.Zn^{2+}$-σ^R complex has a much higher affinity than previously reported[11,28], which is dependent on zinc being bound at the ZAS motif and explains why zinc limitation activates the σ^R regulon in *S. coelicolor*[29]

We next determined the kinetic basis for zinc stabilisation of the complex. Stopped-flow tryptophan fluorescence under pseudo-first order conditions showed that the association rate constant for the $RsrA^{red}$-σ^R complex was only marginally affected by bound zinc, in contrast to the dissociation rate constant which was accelerated 400-fold when zinc was removed (**Figures 3 c and d**). Importantly, the kinetically derived K_d for the $RsrA^{red}.Zn^{2+}$-σ^R complex at 35°C closely matched that obtained by ITC (**Supplementary Table 2**) demonstrating that the kinetic mechanism can simply be described by single association and dissociation rate constants. The kinetically derived K_d at 25 °C (for which a value could not be obtained by ITC) was ~two-fold lower than that at 35°C, with zinc having very similar effects on the kinetics of binding (**Supplementary Table 2**). We conclude that the single ZAS motif zinc ion of RsrA stabilises the high-affinity complex with σ^R by slowing the dissociation rate of the complex.

RsrA is thought to be primarily a sensor of deleterious disulfide bond formation within the *S. coelicolor* cytoplasm since oxidation by the thiol-specific oxidising agent diamide is a stronger inducer of σ^R-dependent promoters than hydrogen peroxide[10]. We therefore determined pre-steady state oxidation rates of $RsrA^{red}.Zn^{2+}$ in complex with σ^R in order to probe the kinetic basis for oxidation, initially using diamide to induce disulfide bond formation within RsrA (**Figure 4a and b**; See Materials and Methods). We developed a stopped-flow spectrophotometric assay to follow $RsrA^{red}.Zn^{2+}$ oxidation, albeit indirectly, by exploiting the absorption changes of diamide on reduction to hydrazine (**Supplementary Figure 2a**)[30].

Zinc release was monitored using the PAR assay (**Figure 4a**). These data showed that the bimolecular rate constant for zinc release is the same as that of diamide reduction (~190 $M^{-1}.s^{-1}$) suggesting zinc release limits the rate of oxidation. This was confirmed by removing zinc from the protein, which accelerated the oxidation rate five-fold (**Figure 4a**). Identical results were obtained for $RsrA^{red}.Zn^{2+}$ in the absence of σ^R demonstrating that complex formation does not influence the kinetics of oxidation (**Supplementary Figure 2c**). Moreover, the release of zinc with increasing diamide concentration showed the oxidant formed a weak intermediate complex (K_1~0.7 mM; **Figure 4b**), most likely the sulfenyl hydrazine (**Supplementary Figure 2a and b**), prior to formation of the trigger disulfide bond. Importantly, the kinetic analysis showed that the first-order rate constant (k_2) for decomposition of this intermediate complex is 0.15 s^{-1} at 25°C. This rate approaches the intrinsic dissociation rate of the RsrA-σ^R complex in the absence of zinc under the same conditions (~0.3 s^{-1}; **Supplementary Table 2**), which is consistent with oxidation increasing the dissociation rate of the complex by driving out bound zinc.

The absorbance of diamide precluded monitoring dissociation of the RsrA-σ^R complex directly by fluorescence spectroscopy. This was however possible using H_2O_2 as an oxidant where the release of zinc could also be monitored (**Figures 4c and d**). Although the bimolecular rate constant for oxidation by H_2O_2 was 500-fold slower than that of diamide (emphasising that RsrA is a sensor of disulfide rather than peroxide stress) here again zinc-release was rate-limiting for oxidation and complex dissociation. Importantly, excess zinc had no effect on the rates of oxidation either by diamide or H_2O_2 (**Supplementary Figure 3 b, c)**, demonstrating that additional zinc ions beyond that bound in the ZAS motif play no role in redox sensing by RsrA. In conclusion, our kinetic data demonstrate that stoichiometric zinc release is the rate-limiting step for RsrA oxidation by different oxidants, which leads to accelerated dissociation of the RsrA-σ^R complex and formation of the trigger disulphide bond (a full kinetic scheme is shown in **Supplementary Figure 3d**).

Importance of the N-terminal ZAS motif cysteine to redox sensing

Heo et al (2013)[31] have suggested that differences in redox sensitivity of different ZAS proteins is due to differences in electronegative residues and binding of alternative zinc ions. However, as our data above illustrate, additional zinc ions play little or no role in the redox sensing ability of RsrA. A simpler explanation for whether ZAS proteins react to disulfide stress is whether the N-terminal zinc-coordinating residue is a cysteine, as in the case of RsrA where Cys11 forms the trigger disulfide with either Cys41 or Cys44. HHCC-type ZAS proteins such as ChrR and RsiW do not have this additional cysteine and do not sense disulphide stress. This hypothesis is confounded however by the recent study of Thakur et al (2010) who reported that on oxidation with hydrogen peroxide, the HHCC ZAS protein RslA from *M. tuberculosis* forms a disulfide bond, expelling the bound zinc and increasing the dissociation rate of the RslA-σ^L complex[22]. We therefore set out to determine how different zinc-ligation chemistries influence oxidative stress sensing, using the RsrA-σ^R complex as a model. We generated four cysteine mutants in RsrA*: RsrA* in which each of the zinc-coordinating cysteines was individually mutated to histidine and RsrA* Cys11His Cys41His Cys44His, in which all the coordinating cysteines were simultaneously replaced with histidine. The latter mutant was used as a non-oxidative control. The Cys-to-His mutations all bound σ^R with lower affinity than wild-type RsrA, the mutations affecting primarily the dissociation rate of the RsrA*-σ^R complex (**Figure 5a and Supplementary Table 1**).

We next challenged RsrA* and all the cysteine mutants with 10 mM H_2O_2 and followed the kinetics of oxidation-induced dissociation of their complexes with σ^R by fluorescence spectroscopy (**Figure 5b**). In contrast to RsrA*, which had similar oxidation-induced dissociation kinetics to wild-type RsrA, neither RsrA* Cys11His nor the triple mutant, RsrA* Cys11His Cys41His Cys44His, oxidatively dissociated when challenged with H_2O_2. However, the single mutants RsrA* Cys41His and RsrA* Cys44His both exhibited identical

oxidation induced dissociation kinetics to RsrA*, consistent with the degeneracy of the trigger disulfide bond (**Supplementary Figure 4)**.

We further analysed RsrA* Cys11His (equivalent to a HHCC motif ZAS protein) in complex with σ^R using high resolution native state nanoelectrospray mass spectrometry to determine the oxidation state of this HHCC-type ZAS protein (**Figure 5c**). Under reducing conditions the RsrA* Cys11His-σ^R complex bound one equivalent of zinc with only a small fraction of apo-complex present. Upon H_2O_2-induced oxidation of the complex a mass shift to lower *m/z* indicated both the loss of zinc and formation of a disulfide bond between Cys41 and Cys44. However, this did not result in oxidation-induced dissociation of the complex (**Figure 5b, c**). These data suggest that oxidative dissociation of a ZAS protein from its target sigma factor requires an N-terminal zinc-coordinating cysteine residue within the ZAS motif (CHCC).

RsrA exposes its hydrophobic core to bind σ^R

In order to understand how RsrA associates with σ^R we determined the structure of zinc-bound RsrA in its reduced state ($RsrA^{red}.Zn^{2+}$) and compared this to a homology model of the $RsrA^{red}.Zn^{2+}$-σ^R complex. A modelling approach was employed because repeated attempts at crystallization of the $RsrA^{red}.Zn^{2+}$-σ^R complex failed to yield diffracting crystals and solution spectra of ^2H, ^{13}C, ^{15}N-labelled $RsrA^{red}.Zn^{2+}$-σ^R complex were poorly resolved. The model was based on previous structures of anti-sigma factor-sigma factor complexes and constrained by bifunctional lysine-specific cross-linking data (**Supplementary Figure 5)**. Following testing of RsrA mutants for optimal spectral resolution (including RsrA*), the NMR solution structure of $RsrA^{red}.Zn^{2+}$ was obtained using the mutant RsrA* Cys41Ser (which contains both Cys11 and Cys44) bound to one equivalent of zinc. As for the wild type protein, ^1H-^{15}N-HSQC NMR spectra showed this mutant required stoichiometric zinc for its stabilization (**Supplementary Figure 6a**). Although RsrA* Cys41Ser likely binds zinc more

weakly than wild type RsrA, leading to weakened σ^R binding (**Supplementary Table 1**), at the protein and zinc concentrations used for NMR structure determination (~mM) the protein is folded and bound to zinc. Only residues 45-47 in RsrA* Cys41Ser could not be assigned by heteronuclear NMR experiments. In the final structure, the N and C-termini, a loop between residues 63 and 72 and residues 42-50 were poorly resolved, all other residues (8-86) were well defined. Heavy atom root mean square deviations (rmsds) for backbone atoms of the secondary structure elements in the 10 overlays of $RsrA^{red}.Zn^{2+}$ shown in **Figure 6b** was 0.48 Å. NMR structure statistics are shown in **Table 1**.

$RsrA^{red}.Zn^{2+}$ (**Figure 6b**) forms a loosely packed four-helix bundle composed of two sets of roughly parallel helices (I-II, residues 11-23 and 29-39 and III-IV, residues 51-60 and 71-84) connected by loops. The two N-terminal helices are tilted ~45° relative to the C-terminal helices. His37 of the conserved ZAS metal binding motif is presented from the C-terminal end of helix II while Cys41Ser and Cys44 are part of the long loop connecting helices II and III. Cys11, the fourth metal ligand, is at the N-terminal end of helix I. The co-localization of the four metal ligands was confirmed by the observation of inter-residue NOEs; distance restraints were used during initial structure calculations and restraints specifying the tetrahedral Zn^{2+} ligation geometry were introduced in the latter stages of refinement (see Materials and Methods).

On binding σ^R $RsrA^{red}.Zn^{2+}$ adopts a characteristic anti-sigma binding domain (ASD) fold, which was first described for the ChrR-σ^E complex[13] (**Figure 7b**). The two key features of the modelled complex are the binding of $RsrA^{red}.Zn^{2+}$ between the two domains of σ^R (σ^2 and σ^4) and the embrace of the sigma factor by the C-terminal helix (helix IV) of $RsrA^{red}.Zn^{2+}$. Our cross-linking data suggest however that helix IV does not adopt a single conformation as in the ChrR-σ^E complex, but can likely contact both σ^2 and σ^4 domains of σ^R (**Supplementary Figure 5c**). For the purposes of the following analysis we focus only on the form of the complex in which helix IV is docked onto the σ^2 domain.

Comparison of the structure of free RsrA^{red}.Zn^{2+} with the σ^{R}-bound state reveals significant structural reorganisation of the anti-sigma factor while maintaining its zinc co-ordination geometry (compare **Figures 7a and b**). (1) The four-helix bundle structure of RsrA^{red}.Zn^{2+} converts to the three-helix ASD fold. This involves helix III changing its orientation by ~90°, helix II by ~30° relative to helix I and helix IV dissociating from the main body of the protein. (2) Helix III in RsrA^{red}.Zn^{2+} approximately doubles in length. The residues comprising this extension were originally the long loop connecting helices II and III in RsrA^{red}.Zn^{2+}. As a consequence, Cys44 of the ZAS motif becomes part of helix III while Cys41 sits between helices II and III. The other ZAS motif residues remain within their original secondary structure elements. The orientation of the extended helix III is dictated by Cys44's role in zinc co-ordination, emphasizing the importance of zinc in σ^{R} binding as it allows the helices of RsrA to re-organise around the metal ion. Importantly, the extended regions of helix III no longer pack against helices I & II of RsrA^{red}.Zn^{2+} as in the free state. Exposed hydrophobic residues in the C-terminal half of helix III (Leu50, Ala53, Val54 and Leu57), which were originally part of the hydrophobic core in the free RsrA^{red}.Zn^{2+} state, now interact with σ^{R}. Conversely, hydrophobic residues (Leu45 and Tyr48) that were part of the loop between helices II and III in the unbound state and partially solvent exposed now form part of the hydrophobic core of RsrA^{Red}-Zn^{2+} in its σ^{R}-bound state. (3) The telescopic extension of helix III projects helix IV away from the body of RsrA allowing the anti-sigma factor to wrap around σ^{R}. (4) Hydrophobic residues within helix IV of RsrA, specifically Val75 and Leu79, which were peripheral hydrophobic core residues in RsrA^{Red}-Zn^{2+}, now make contact with the sigma factor. (5) Several of the bulky residues from RsrA's hydrophobic core which bind σ^{R} (Val54, Leu57, Val75 and Leu79) are conserved or conservatively substituted within the ZAS protein family suggesting they serve similar roles in all ZAS proteins (**Figure 7d**). The contact sites of these hydrophobic residues on σ^{R} are consistent with their blocking important interactions of the sigma factor with RNA polymerase, as originally described by Campbell et al (2007)[13]. (6) RsrA double alanine mutants (Val54Ala Leu57Ala and Val75Ala Leu79Ala) each weakened binding to σ^{R} by

>100-fold, consistent with their making stabilising contacts with the sigma factor (**Supplementary Table 1**). In summary, the loosely packed four-helical bundle structure of $RsrA^{red}.Zn^{2+}$ undergoes large-scale structural remodelling on binding σ^R while maintaining the same ligation chemistry of the ZAS motif zinc ion. These conformational changes open up the structure of $RsrA^{red}.Zn^{2+}$ and enable its embrace of σ^R using hydrophobic residues released from its hydrophobic core.

RsrA sequesters its σ^R-contacting residues on oxidation

We next determined the structure of oxidized RsrA ($RsrA^{ox}$) to understand how this blocks σ^R binding. We first ascertained which of the two oxidised forms of the trigger disulphide predominate at equilibrium (**Supplementary Figure 6 and 7**). These experiments focused on RsrA*, which behaves as a redox sensor *in vivo*[23] and *in vitro* (**Figure 5b**). RsrA* Cys11-Cys44 was found to be the most populated oxidised state. We therefore determined the solution structure of oxidized RsrA* containing the Cys11-Cys44 disulfide bond. Cys41 was mutated to serine in this construct to remove the potential for mixed disulfide bond formation (see Materials and Methods). As with $RsrA^{red}.Zn^{2+}$, the N-termini of $RsrA^{ox}$ were disordered and the loop between residues 63 and 72 poorly defined. Heavy atom rmsds for the top 10 solution structures of residues 8-86 in $RsrA^{ox}$ were 0.38 Å (**Figure 6c**; **Table 1** for structure statistics).

^1H-^{15}N HSQC spectra of $RsrA^{red}.Zn^{2+}$ and $RsrA^{ox}$ are substantially different suggestive of distinct folds (**Figure 6a**). This is confirmed by the structure of $RsrA^{ox}$, which is more helical than $RsrA^{red}.Zn^{2+}$ (**Figures 6b and c**). $RsrA^{ox}$ is also more compact than $RsrA^{red}.Zn^{2+}$, with 13% less solvent accessible surface area ($RsrA^{Red}$-Zn^{2+}, 2608±28 $Å^2$ and $RsrA^{ox}$, 2270±33 $Å^2$ for residues 8-86). Helices I (residues 13-24) and II (residues 31-40) are pulled closer together by the disulfide between Cys11 and Cys44 and helices III^C (50-60) and IV (70-84) reorient to become roughly parallel to those of helices I and II. An additional

short helix (helix III^N; residues 42-48), perpendicular to the other helices and stabilised by the disulfide, takes the place of the ZAS metal-binding site. Indeed, residues comprising helix III in $RsrA^{ox}$ are equivalent to those in the σ^R-bound state of RsrA but now the helix is broken into two segments, a 90° one-residue turn connecting helices III^N and III^C (**Figure 7 b-d**).

These changes have three major consequences. (1) The zinc-binding site of $RsrA^{red}.Zn^{2+}$ is obliterated; this is most readily appreciated by the distance between NE2 atom of His37 and the S atom of Cys11 (15 Å) (**Figures 6b and c**). (2) The movement of ZAS ligands away from the metal binding site is brought about by a change in register of helix II relative to the other helices due to a rotation around the helix axis. (3) The trigger disulfide bond constrains the orientations of helices I II along with III^N and III^C, resulting in wholesale repacking of its hydrophobic core.

The remodelling of the hydrophobic core is exemplified by changes associated with the reorientation of His37 (**Figures 7 a-c**). In $RsrA^{red}.Zn^{2+}$, zinc ligation by His37 necessitates rotation of Phe38 out of the hydrophobic core. In $RsrA^{ox}$, Phe38 (helix II) interacts with Val54 (helix III^C) and Leu18 and Phe21 (Helix I) within the hydrophobic core of the protein, which keeps helix III^C packed onto helices I & II and so blocking RsrA's ability to interact with σ^R. Moreover, Val75 in helix IV also forms hydrophobic contacts with residues in $RsrA^{ox}$ (Leu18, Val54 and Leu57). Hence, formation of the trigger disulfide between Cys11 and Cys44 propagates collapse of the σ^R-bound form of RsrA, blocking the structural reorganisation required for extension of helix III and release of helix IV. The consequence of these structural changes is that σ^R-contacting residues are sequestered back into RsrA's hydrophobic core.

The structure of $RsrA^{ox}$ explains why the Cys41-Cys44 disulfide does not cause dissociation of the complex. Whereas a disulphide between Cys11 and Cys44 pins helices I and III^N together, stabilising the hydrophobic core and sequestering key hydrophobic residues away from σ^R, a disulphide between Cys41 and Cys44 places no constraints on

helix I. Hence, RsrA with the Cys41-Cys44 disulfide is still able to expose its hydrophobic core in order to bind σ^R. This in turn explains why Cys11 is required for redox sensing. Finally, the structure of $RsrA^{ox}$ explains why the trigger disulfide is degenerate since the sidechains of Cys41Ser and Cys44 are presented to Cys11 from consecutive turns of helix III^N such that they can both form a disulphide bond (**Figure 7c**). The similarity of the HSQC spectra of the two oxidized forms of RsrA (Cys11-Cys41 and Cys11-Cys44**; Supplementary Figure 6b**) further suggest their structures are likely to be similar.

Discussion

The mechanisms by which sensor proteins respond to oxidative stress in bacteria are varied but fall broadly into two groups, those that contain metal centres such as the transcriptional repressor PerR[32] and chaperone Hsp33[33], and those that have reactive cysteines, such as the transcription factors OxyR[34] and OhrR[35]. Oxidation of tetrameric OxyR by hydrogen peroxide induces disulfide bond formation within OxyR monomers, the resulting conformational changes converting it from a transcriptional repressor into an activator[36]. The OhrR family of dimeric transcriptional repressors are derepressed by organic hydroperoxides following oxidation either of a single reactive cysteine or through intersubunit disulfide bond formation[35,37]. The dimeric transcriptional repressor PerR contains two metal centres, a structural Zn^{2+} site containing histidine residues[32], and a regulatory site which in its Fe^{2+}-bound state is responsive to oxidation. Derepression of PerR by hydrogen peroxide occurs through oxidation of metal binding histidine residues following the generation of HO· by Fenton chemistry at the Fe^{2+} site. Hsp33 is a heat shock protein that becomes activated during oxidative stress. A single zinc ion is coordinated by four cysteines in the C-terminal domain of Hsp33. Following oxidation with H_2O_2, intramolecular disulfide bonds form between the zinc-ligating cysteines, expelling bound zinc and forming a dimeric chaperone[38]. Zinc is also expelled from $RsrA^{red}.Zn^{2+}$ on oxidation to $RsrA^{ox}$, but in this instance release of zinc accelerates the dissociation rate of its complex with σ^R prior to formation of the trigger disulphide bond between its zinc-coordinating cysteine residues. Intriguingly, $RsrA^{red}.Zn^{2+}$ has the same redox potential as OxyR[39] even though the two proteins share no structural similarity and sense different oxidative stresses by completely different mechanisms. Finally, RsrA is the first example of an oxidative stress sensor that responds to oxidation by sequestering hydrophobic residues required to stabilise the protein-protein interaction with its cognate transcription factor back into its own hydrophobic core. The same residues are involved in stabilising three distinct structural states of the anti-sigma factor, $RsrA^{red}.Zn^{2+}$, $RsrA^{red}.Zn^{2+}$-σ^R complex and $RsrA^{ox}$ (**Figure 7**).

$RsrA^{red}.Zn^{2+}$ and $RsrA^{red}.Zn^{2+}$-σ^R complex are equally reactive towards oxidants however given the high affinity of the complex (K_d ~ 0.7 nM) and the co-expression of their genes in *S. coelicolor* it is likely that the complex is the redox sensor. The distance between the sulfur atoms of Cys11 and Cys44 in the metal binding site is ~3.5 Å for both $RsrA^{red}.Zn^{2+}$ and the $RsrA^{red}.Zn^{2+}$-σ^R complex. Formation of a disulfide bond between these sulfur atoms reduces the interatomic distance to 2.05 Å. This small (~1.5 Å) change in bond length and valency precipitates a ~20 Å contraction of the σ^R-bound state to form $RsrA^{ox}$. Hence, oxidation of the RsrA thiols represents a highly efficient means of amplifying a small, local, chemical change into a large-scale structural collapse that blocks binding to σ^R.

Campbell et al (2007)[13] have previously defined an anti-sigma domain (ASD) fold for both zinc-binding and non-zinc binding anti-sigma factors. It is clear from the present work that this fold pertains only to the sigma-bound states of anti-sigma factors. The structure of $RsrA^{red}.Zn^{2+}$ illustrates a very different four-helix bundle structure when not bound to its cognate sigma factor. We term this form of the anti-sigma factor the ZAS fold (**Supplementary Figure 8**). Structure-based sequence alignments of ZAS proteins recovered from bacterial genomes show that in addition to the zinc-binding ZAS motif these proteins all share conserved or conservatively substituted hydrophobic residues. Those displayed from helices I and II stabilise the ZAS and ASD folds of RsrA while those displayed from helices III and IV stabilise the ZAS fold in the absence of sigma factor but are then recruited to bind the sigma factor (**Supplementary Figure 8b**).

A poorly understood feature of bacterial ZAS proteins is that they respond to diverse stresses. The present work shows why ZAS proteins with HHCC-type sequence motifs cannot be sensors of disulphide or peroxide stress, implying that additional domains or sequences are involved in sensing other types of stress. This is the case for the HHCC-type ZAS protein ChrR from *R. sphaeroides* where its cupin-like domain is the sensor of singlet oxygen stress. Sequence surveys of the ZAS sequence motif identifies >1100 ZAS proteins distributed widely amongst bacterial phyla (**Supplementary Figure 8 b, c**). We found a statistically significant correlation of HHCC-type ZAS proteins with cupin-7 domains (66/498

HHCC-type ZAS sequences versus 1/665 CHCC-type ZAS sequences). How additional sensor domains disrupt the protein-protein interactions of ZAS protein-sigma factor complexes is unknown. We speculate that the modulation by zinc of the binding affinity of these complexes may be a route by which diverse signals could result in ZAS protein dissociation from the sigma factor. Zinc dissociation could be brought about by destruction of zinc ligands by ROS, as occurs in the transcriptional repressor PerR, or proteolytic cleavage, as occurs in the ZAS protein RsiW[40].

Materials and Methods

Protein purification

RsrA and its mutants were expressed and purified from *E. coli* BL21(DE3) pLysS using a His-tag that was subsequently removed by thrombin cleavage. $RsrA^{ox}$ was generated by treating the protein with 0.1 mM diamide for 30 min. The reduced and oxidised forms of the proteins for structure determination were prepared on a Vydac C8 semi-preparative HPLC column; Buffer A was 5% acetonitrile, 95% H_2O, 0.1% trifluoroacetic acid (TFA) and Buffer B was 95% acetonitrile, 5% H_2O, 0.1% TFA. Zinc reconstitution of reduced RsrA is described below. Uniformly ^{15}N-labelled and ^{15}N,^{13}C-labelled protein was prepared using minimal growth media supplemented with ^{15}N ammonium chloride and ^{13}C glucose (Cambridge Isotope Laboratories). σ^R was purified without using purification tags. Residues 5-227 were subcloned into pET21a using NdeI and BamHI restriction sites with a C-terminal stop codon to enable tagless expression of σ^R. σ^R in pET21a was expressed in *E. coli* BL21(DE3) cells at 37°C in LB and expressed with 1 mM IPTG for 3 h post induction. Cells were harvested by centrifugation and lysed by sonication in 50 mM Tris pH 7.5, 100 mM NaCl. Lysate was purified by centrifugation and the supernatant further purified by ammonium sulphate precipitation. σ^R precipitated at 40% saturation ammonium sulphate. The pellet was resuspended in 50 mM Tris pH 7.5, 10 mM NaCl and loaded onto a Q-Sepharose column. Purified σ^R was concentrated and then loaded onto Hi-Load S75 column and eluted in 50 mM Tris pH 7.5, 100 mM NaCl. All σ^R mutants were similarly purified . $RsrA^{red}.Zn^{2+}$-σ^R complexes were generated by co-expressing the two genes in the same expressing strain of *E. coli*. *sigR* was cloned into pCDF-DUET1 vector between the BamHI and HindIII in MCS1. pET15b-*rsrA* and pCDF-DUET1-*sigR* were co expressed in pLysS-Rosetta2 cells. Protein was purified using the N-terminal histidine tag of RsrA on a Ni^{2+}-charged NTA column and then subsequently purified by size exclusion chromatography using a Superdex-75 column.

Site directed Mutagenesis

Mutations were made using the QuickChange lightning Multi Site-Directed mutagenesis kit (Agilent) following the manufacturer's instructions. Primer sets were purchased from MWG-Biotech (UK). Introduction of mutations were confirmed by DNA sequencing (Source Biosciences).

Stoichiometry of zinc binding to RsrA

Controversy surrounds the role of zinc in RsrA function. Li et al (2003)[25] and Bae et al (2004)[26] have suggested that zinc has little role to play in σ^R binding and redox sensing, respectively, while Heo et al (2013) suggest multiple zinc ions bind to RsrA to modulate its redox reactivity[31]. We re-assessed the stoichiometry of zinc binding prior to dissecting the redox sensing mechanism. Using both wild type RsrA and RsrA*, in which the four non-essential cysteines (Cys3, Cys31, Cys61 and Cys62) were mutated to alanine, native state nanoelectrospray mass spectrometry showed that both proteins in the reduced state bind multiple zinc ions (**Supplementary Figure 1a** shows data for the wild type protein). Zinc titrations using RsrA* in circular dichroism and mass spectrometry experiments indicated that only a single zinc ion is required to stabilise the RsrA fold (**Supplementary Figure 1 a-d**). Previous estimates of the affinity of RsrA for zinc documented an equilibrium dissociation constant (K_d) of ~10^{-17} M [26], which is reasonable to assume pertains to this structural metal ion. We refer to this reduced, zinc-bound state of RsrA as $RsrA^{red}.Zn^{2+}$. This form of RsrA (dissolved in 50 mM Tris pH 7.5, 100 mM NaCl, 1 mM DTT) was obtained by treating all preparations of the protein with EDTA (1 mM, 15 min incubation), followed by desalting on a HiTrap column (5 ml) and, unless specified, stoichiometric zinc (Alfa Aesar, 99,9% purity) added back to the protein.

Fluorescence spectroscopy

Changes in the intrinsic tryptophan fluorescence emission of σ^R on binding $RsrA^{red}.Zn^{2+}$ were monitored using a Horiba FluoroMax4 spectrofluorimeter in 50 mM Tris pH 7.5 buffer containing 100 mM NaCl and 2 mM DTT at 25°C. Samples were excited at 295 nm and emission spectra recorded from 310 to 450 nm. Experiments were conducted using 3 nm slit widths. σ^R was kept at 1 µM and the concentration of RsrA varied from 0.1 to 2 µM from which the fractional change in fluorescence change was determined.

Circular dichroism spectroscopy

Apo-RsrA was prepared by incubating the protein with 1 mM EDTA for 15 minutes at 4˚C before buffer exchanging to the experimental buffer using a HiTrap column. Samples were incubated in 50 mM Tris pH 7.5 buffer containing 100 mM NaCl and 2 mM DTT before desalting in 10 mM Tris pH 7.5 buffer using a Hi-Trap column. Experiments were conducted immediately on a Jasco-J815 CD spectrometer at 20˚C using a 1 mm path length cuvette. Data collected as ellipticity in millidegrees were converted to mean residue ellipticity, [θ] (degrees.cm^2/dmol.residue).

Native state mass spectrometry of protein complexes

Intact mass spectrometry measurements were performed on a Waters Synapt G2 HDMS modified for high mass transmission[42]. Samples were buffer exchanged into 25 mM ammonium acetate using Bio-Spin 6 (Bio-Rad) columns prior to MS analysis. Typically, each measurement was performed by loading 3 µL of protein sample into gold-coated nanospray capillaries prepared in-house[43] and loaded into a static nanospray block providing the spray voltage. Electrospray was induced by applying a potential of between 0.9 – 1.2 kV to the capillary. A sample cone of 50 V was used to capture the charged droplets, with a

source backing pressure of 5.5 mbar. The instrument was operated in TOF mode (no IMS separation), with the trap and transfer collision cells held at an acceleration voltage of 10 and 5 V respectively (with an argon pressure of $2x10^{-2}$ mbar). Data were processed using the MassLynx software. For high-resolution MS measurement, utilised to measure the presence/absence of the disulphide in the RsrA* Cys11His σ^R complex, a Thermo Scientific Q-Exactive hybrid quadrupole-Orbitrap mass spectrometer was used. The instrument was modified for high mass measurement as described elsewhere[44,45] and optimised for retention of non-covalent interactions. Hardware alterations include a lower RF frequency applied to the selection quadrupole and a gas line allowing higher pressures to be achieved in the HCD cell. The instrument was operated in "Native Mode" where both the RF frequencies applied to transfer optics and Orbitrap voltages were optimised for high mass species. Ions were generated in the positive ion mode from a static nanospray source using gold-coated capillaries prepared in-house, then passed through a temperature controlled transfer tube (set to 20°C, readback 31°C), RF-lens, injection flatapole and bent flatapole. After traversing the selection quadrupole, which was operated with a wide selection window (1,000-10,000 m/z), ions were trapped in the HCD cell before being transferred into the C-trap and Orbitrap mass analyser for detection. Transient times were 128 ms (35,000 at m/z=200) and AGC target was 1×106 with a max fill time of 100ms. No additional HCD or in-source activation was applied. Argon was used as the collision gas and the pressure in the HCD cell was maintained at around 1.3×10-9 mbar. In order to achieve both representative mass measurement and good separation of the bound species, approximately 100 spectra, each of 25 microscans, were acquired then averaged using Thermo Scientific Xcalibur 2.1. Masses were calculated using the three most abundant charge states using an in-house software tool. Calibration was performed prior to mass measurement up to 11,300 m/z using clusters of CsI.

Redox potential measurements

The redox potential of the $RsrA^{red}.Zn^{2+}$-σ^R complex was determined with reference to a GSH-GSSG (glutathione-glutathione disulfide) redox couple and monitoring the change in tryptophan fluorescence emission at 343 nm (excitation at 295 nm) of the complex (see above) and at 500 nm using the PAR assay in a spectrophotometer to determine the fraction of dissociated zinc (see below). Glutathione and glutathione disulfide were from Sigma Aldrich. Fluorescence titration experiments were carried out in 50 mM Tris pH 7.5 buffer and 100 mM NaCl at 25˚C. All buffers were degassed and purged with N_2 gas prior to use. In all experiments, GSH was kept constant at 0.5 µM while GSSG was varied from 100 µM to 100 mM. The $RsrA^{red}.Zn^{2+}$-σ^R complex was at 2 µM. All samples were incubated with the redox couple for 2 h before data collection. 2 h was deemed as having reached equilibrium since longer incubations had no effect. Data were corrected for the inner-filter effect, as described[46]. Inclusion of the PAR reagent does not influence redox titration experiments since its affinity for zinc is several orders of magnitude lower than that of RsrA[47]. Positive and negative controls were collected at each redox couple concentration. Positive controls had 1 equivalent Zn^{2+} along with the PAR reagent and the GSH couple. Negative controls had the couple and PAR. The difference between the positive and the negative control gave the total signal change for that concentration of redox couple. Ratio of the experiment over the total signal change gave the ratio of zinc released. The fraction of $RsrA^{red}.Zn^{2+}$-σ^R complex dissociated and the fraction of zinc released were used to determine the fraction of reduced RsrA (R). The variation of reduced RsrA against $\frac{[GSH]^2}{[GSSG]}$ was fitted to equation 1 to determine K_{eq} in M units. K_{eq} thus obtained was used in the Nernst equation (equation 2) to calculate RsrA's redox potential.

$$R = \frac{\frac{[GSH]^2}{[GSSG]}}{K_{eq}+\left(\frac{[GSH]^2}{[GSSG]}\right)} \qquad \text{eq (1)}$$

where R is the reduced fraction of RsrA.

$$E_0^{RsrA} = E_0^{GSH/GSSG} - \left(\frac{RT}{2F}\right) \text{x } \ln K_{eq} \quad \text{eq (2)}$$

where E_0^{RsrA} is the redox potential of RsrA. $E_0^{GSH/GSSG}$ is the redox potential of glutathione, which is -240 mV at 25 ˚C, pH 7.5[48]. R is the gas constant 8.314 J K^{-1} mol^{-1} and F is the Faraday constant, 96.485 J mV^{-1} mol^{-1}.

ITC measurements

All experiments were conducted using a Microcal ITC_{200} instrument at 35°C in 50 mM Tris pH 7.5 buffer containing 100 mM NaCl and 2 mM DTT. No heats of binding could be detected at 25°C. The affinity of the $RsrA^{red}.Zn^{2+}$-σ^R complex was too high to be determined by direct titration and so was obtained by competition ITC. A weak binding mutant of RsrA, RsrA* Cys11Ser Cys44Ser (K_d, 185 nM), was included in the cell with σ^R as a competitor. $RsrA^{red}.Zn^{2+}$ was titrated into this mixture. For weaker binding mutants of RsrA or in experiments where zinc was omitted thermodynamic data were obtained by direct titration where 10 µM RsrA was in the cell and 100 µM σ^R in the syringe. Where zinc was included in the experiment, RsrA was pre-incubated in 50 mM Tris pH 7.5, 100 mM NaCl, 10 mM DTT, 1 mM $ZnCl_2$ and then buffer exchanged on a 5 ml Hi-Trap column into 50 mM Tris 7.5, 100 mM NaCl and 2 mM DTT. Zinc could not be included in the cell due to precipitation of σ^R during the titrations. All experiments were carried out immediately after buffer exchange and in triplicate. Averages and standard deviations of the obtained parameters are reported from triplicate experiments. Data were analysed using the manufacturer's software assuming a single binding site model. Competition ITC titrations were performed at the same temperature and in the same buffer conditions by injecting 100 µM RsrA into 10 µM σ^R

containing 50 μM RsrA* Cys41Ser. Binding isotherms were analysed using the manufacturer's software for a competitive binding model[49].

Association and dissociation kinetics of the RsrA-σ^R complex

Association Kinetics Stopped-flow fluorescence experiments were performed on an Applied Photophysics SX20MV instrument setup for 1:1 single mixing and thermostated using a circulating water bath. An excitation wavelength of 295 nm was used for the excitation of σ^R's two tryptophans (RsrA does not contain tryptophan), while a 320 nm filter was used to collected the fluorescence emission. The manual entrance and exit slits were set to 2 mm (Bandpass = 4.65 nm / mm). Experiments were carried out at 25°C or 35°C in 50 mM Tris pH 7.5 buffer containing 100 mM NaCl and 2 mM DTT. RsrA was pre incubated in 50 mM Tris 7.5, 100 mM NaCl, 10 mM DTT, 1 mM $ZnCl_2$ and buffer exchanged using a 5 ml Hi-Trap column into 50 mM Tris pH 7.5, 100 mM NaCl and 2 mM DTT prior to use. All association experiments were done under pseudo-first order conditions. The concentration of σ^R was kept constant at 125 nM and RsrA (± Zn^{2+}) varied from 1.25 μM to 2.5 μM in 250 nM increments. The kinetic traces were fitted to a single-exponential rate equation by nonlinear least square regression on the manufacturer's software. Values of k_{obs} were then plotted against RsrA concentration to determine the bimolecular association rate constant (k_{on}). Data presented are averages of three traces in each stopped-flow experiment and each experiment was performed three times. Quoted errors are the standard deviation from the three repeats. Apo-RsrA was prepared by incubating the protein with 1 mM EDTA for 15 minutes at 4˚C before buffer exchanging to the experimental buffer on a HiTrap column.

Dissociation kinetics Competition experiments were conducted to determine the dissociation rate constant of the RsrA-σ^R complex by mixing 2.5 μM $RsrA^{red}.Zn^{2+}$-σ^R complex with 25 μM σ^R Trp88Ile Trp119Ile. σ^R Trp88Ile Trp119Ile binds $RsrA^{red}.Zn^{2+}$ with the same affinity as wild-type σ^R (**Supplementary Figure 3a**) but does not produce a change in tryptophan

fluorescence. All experimental conditions were as described above. The dissociation trace was fitted to a single exponential rate to determine k_{off}. All experiments were repeated three times and averages and standard deviations reported. Apo-RsrA was prepared as described above. Zinc-bound-RsrA was prepared by incubating either 1 or 3 equivalents of Zn^{2+} for 15 minutes at 4˚ C before buffer exchanging to the experimental buffer on a HiTrap column.

Oxidation kinetics of the RsrA-σ^R complex

All experiments were conducted at 25°C in 50 mM Tris pH 7.5 buffer containing 100 mM NaCl. Buffers were thoroughly degassed and purged with N_2 gas before use.

Oxidation by diamide The reaction of diamide with thiols can be followed spectrophotometrically at 320 nm. Each diamide molecule oxidises two thiols forming a disulfide and in the process diamide is converted from its diazene to hydrazine form (**Supplementary Figure 2**). Only the diazene form absorbs at 320 nm[30]. For second order experiments, diamide (25 μM) was added to $RsrA^{red}.Zn^{2+}$-σ^R complex (25 μM), prepared by incubating EDTA treated complex with 1 equivalent Zn^{2+}. Oxidation of the complex (± Zn^{2+}) was followed by the change in absorbance at 320 nm for 1200 s using an Applied Photophysics SX20MV stopped-flow apparatus. The concentration of diamide at various time points was computed by determining the ratio of diamide consumed relative to a control in which 25 μM diamide was converted to the hydrazine form using 500 μM DTT. Raw data were then linearized by plotting the variation of 1/[diamide] against time from which the second order rate constant for diamide-induced oxidation was determined. Zinc release from the $RsrA^{red}.Zn^{2+}$-σ^R complex on oxidation with diamide was measured using 100 μM PAR (4-(2-Pyridylazo) resorcinol), which absorbs at 500 nm on zinc binding[47]. The second order rate of diamide-induced release of Zn^{2+} was determined as described above using the PAR assay. For pseudo-first order experiments, only zinc release was monitored from the

$RsrA^{red}.Zn^{2+}$-σ^R complex (2 μM), where diamide was varied from 25 μM to 20 mM. Traces were fitted to a single exponential rate equation to obtain the observed Zn^{2+} release rate, $k_{obs.}$ Plots of k_{obs} versus diamide concentration were hyperbolic, the data fitted to the Michealis-Menten equation from which values for K_1 and k_2 were extracted (**Supplementary Figure 2b**). The average and standard deviations reported are from triplicate experiments.

Oxidation by H_2O_2 Buffer and experimental conditions were as described above. Only pseudo-first order experiments were conducted with H_2O_2. Zinc release was monitored in a stopped-flow apparatus using the PAR assay where the $RsrA^{red}.Zn^{2+}$-σ^R complex (2 μM) was incubated with varying concentrations of H_2O_2 (1-10 mM). PAR was kept at 100 μM. Observed rates of Zn^{2+} release were plotted against the concentration of H_2O_2 from which the bimolecular rate constant was obtained as above. The change in intrinsic tryptophan fluorescence of σ^R on complex formation was also exploited to follow the rate of complex dissociation on treatment with H_2O_2. $RsrA^{red}.Zn^{2+}$-σ^R complex (2 μM) was incubated with varying concentrations of H_2O_2 (1-10 mM) and the extent of complex dissociation determined by fluorescence spectroscopy (excitation wavelength, 295 nm, emission wavelength, 343 nm) using a Fluoromax-4 spectrometer and 10 mm pathlength quartz cuvettes. The average and standard deviations reported are from triplicate experiments.

Cross linking-based homology modelling of the $RsrA^{red}.Zn^{2+}$-σ^R complex

Crosslinking was used to constrain homology models of the complex. 5 μM purified $RsrA^{red}.Zn^{2+}$-σ^R complex in 20 mM Hepes pH 7.5 buffer containing 50 mM NaCl and 2 mM DTT was incubated with 2 mM of 1:1 mixture of BS2G-d_0 and BS2G-d_4 (bis(sulfosuccinimidyl) 2,2,4,4-glutarate) or 1:1 mixture of BS3-d_0 and BS3-d_4. Cross-linking reactions were allowed to take place at room temperature for 30 minutes, and then quenched with Tris-HCl pH 7.5 to a final concentration of 100 mM. Samples were then separated on 15 % SDS-PAGE and cross-linked bands excised, reduced with 10 mM DTT at

56ºC for 30 minutes, and alkylated with 50 mM iodoacetamide (Sigma-Aldrich) in the dark at room temperature for 20 minutes. 10 ng/uL trypsin (Porcine, Promega) was then added to cover gel pieces and digestion was allowed to continue overnight at 37ºC while shaking. Tryptic peptides were separated on an EASY-nLC[50] 1000 UHPLC system (Proxeon) and electrosprayed directly into a Q Exactive mass spectrometer (Thermo Fischer Scientific) through an EASY-Spray nano-electrospray ion source (Thermo Fischer Scientific). Peptides were trapped on an in-house packed guard column (75 µm i.d. x 20 mm, reprosil C18, 3µm, 120 Å) using solvent A (0.1% Formic Acid in water) at a pressure of 500 bar and then fractionated using an EASY-spray Acclaim PepMap® analytical column (75 µm i.d. × 500 mm, RSLC C18, 2 µm, 100 Å) eluted with a linear gradient (7 % to 31 % solvent B (0.1% formic acid in acetonitrile in 30 min) at a flow rate of 200 nL/min. Full scan MS spectra were acquired in the Orbitrap (scan range 350-2000 m/z, resolution 70000, AGC target 3e6, maximum injection time 100 ms). After the MS scans, the 10 most intense peaks were selected for HCD fragmentation at 30 % of normalised collision energy. HCD spectra were also acquired in the Orbitrap (resolution 17500, AGC target 5e4, maximum injection time 120 ms) with first fixed mass at 100 m/z. Charge states 1+ and 2+ were excluded from HCD fragmentation.

MS data were converted into mgf format using MSconvert from the ProteoWizard toolbox[51] and searched using the pLink software[52]. The database contained the target proteins only (RsrA and σ^R). Search parameters were as follows: maximum number of missed cleavages = 2, fixed modification = carbamidomethyl-Cys, variable modification 1 = Oxidation-Met, variable modification 2 = Glu to pyro-Glu, mass shift of BS2G_d_0 = 96.02113, mass shift of BS2G-d_4 = 100.04583, mass shift of BS3-d_0 = 138.06809, mass shift of BS3-d_4 = 142.09279, mass accuracy filter = 20 ppm for precursor ions with consideration of the first 5 isotopic peaks, MS2 tolerance = 20 ppm. Data were initially filtered by E-value (E<1.98e-4). Cross-links were further inspected by checking the presence of the peak pair in the MS spectra generated by the d_4/d_0 mixture, as well as fragmentation patterns.

Three initial atomic models of RsrA-σ^R complex were built based on the crystal structures of RseA-σ^E (ref.53), ChrR-RpoE[13] and RslA-σ^L (ref.22) using MODELLER V9.12[54]. Structure based alignment of the above three models with the NMR structure of $RsrA^{red}.Zn^{2+}$ was used to define the secondary structure of RsrA in the complex. Each model was checked against the experimental cross-links. A model based on RseA-σ^E alone did not satisfy the cross-links observed and hence discounted while the pattern of crosslinks discounted the conformational change seen for σ^4 in the ChrR-RpoE complex[13]. A final composite model was built for σ^R using the crystal structures of the σ^2 domain from σ^R (ref.41) and σ^4 domain from the RslA-σ^L (ref22) complex, and for $RsrA^{red}.Zn^{2+}$ from ChrR and RslA from their complexes with σ^E/RpoE and σ^L, respectively. Lysine residues from helix IV of RsrA gave cross-links to different regions of σ^R consistent with previous observations that it can exist in different conformations in ZAS protein complex structures, contacting either the σ^2 or σ^4 domains[13]. One hundred models were generated and the lowest energy model (assessed by DOPE energy function) selected for further analysis.

NMR Spectroscopy

RsrA* Cys41Ser concentrations in all NMR samples were 1-1.5mM. Oxidized samples were prepared in 20 mM Tris-HCl (pH 7.1) 95% H_2O/5% D_2O. For reduced state samples, spectra were acquired in 20 mM Tris-HCl (pH 7.1), 5 mM dithiothreitol (DTT), 2mM $ZnCl_2$, 95% H_2O/5% D_2O. Where necessary (eg. for acquisition of homonuclear two-dimensional NOESY and TOCSY experiments) deuterated Tris and DTT (Cambridge Isotope Laboratories) were used. With the exception of experiments to measure residual dipolar couplings (RDCs; see below), all the NMR experiments were performed on a Bruker Ultrashield 700 MHz spectrometer with triple (^1H, ^{15}N, ^{13}C) nucleus (TXI, Bruker Biospin) probe equipped with z gradient coils, running TopSpin (Bruker BioSpin) software and belonging to the University of York Centre for Magnetic Resonance. All experiments were

performed at 298K with NOESY mixing times of 100-150ms and a TOCSY mixing time of 50ms.

Processing and Assignment of NMR Spectra All spectra were processed using NMRPipe[55]. Backbone and sidechain assignments were made using a standard suite of three-dimensional (3D) triple resonance experiments HNCA, CBCANH and CBCA(CO)NH, HNCO and HN(CA)CO in addition to 3D ^{15}N-^{1}H HSQC-NOESY and ^{15}N-^{1}H HSQC-TOCSY. NOEs were assigned using 3D NOESY and 2D ^{1}H-^{1}H NOESY experiments. Assignments were made using CcpNmr Analysis version 1.0[56]. Chemical shift assignments were deposited at BMRB (accession numbers 25955 and 25956 for RsrA^{red}.Zn^{2+} and RsrA^{Ox} respectively).

Residual Dipolar Couplings (RDCs). The ^{1}H-^{15}N RDCs[57] were recorded using anti-phase/in-phase experiments[58] at 14 T (^{1}H larmor frequency of 600 MHz) at the University of Southampton using a 5% C12E6/hexanol (r=0.64) liquid crystalline medium as an alignment medium[59]. Data in the isotropic and aligned state for both the RsrA^{red}.Zn and RsrA^{ox} samples were acquired at 298K with sweep widths of 10000 Hz and 1800 Hz, and acquisition times of 51 ms and 100 ms, for ^{1}H and ^{15}N, respectively. The observed deuterium splitting in the aligned state was 24 Hz for both the zinc-bound and oxidised samples. The data were processed with NMRPipe[55] and were further analysed with Sparky[60] using the built-in peak fitting module to determine the peak positions. Errors were estimated to be 1Hz. The RDCs (40 restraints for RsrA^{ox} and 29 for RsrA^{red}.Zn^{2+}) were analysed using Module[61] and incorporated into the structure calculations during refinement.

Structure Calculation and Validation One hundred structures were calculated using the program CNS[62] (**Table 1**). The Ser42-Pro43 peptide bond was modelled in the *cis* conformation (using the CIPP patch) in the structure of RsrA^{red}.Zn, based on the presence of an NOE between the Hα atoms of Ser42 and Pro43 and between Hβ of Ser42 and Hα of Pro43 and on the lack of NOEs between Ser42 Hα and Pro43 Hδ that would be

characteristic of a *trans* conformation. In $RsrA^{ox}$ however this bond was modelled in the *trans* conformation based on observed NOEs between Ser42 Hα and Pro43 Hδ. An additional patch was generated for inclusion of the zinc atom and modification of the zinc ligands (Cys11, His37, Cys41Ser and Cys44) in $RsrA^{red}$.Zn. Estimates of backbone dihedral angles were obtained using TALOS[64]; only restraints for residues that had "good" predictions were included. Accessible molecular surface areas on a per residue basis (averaged over the 10 lowest energy structures for $RsrA^{red}.Zn^{2+}$ and $RsrA^{ox}$) were calculated using WHAT IF[65]. Structure coordinates of $RsrA^{ox}$ and $RsrA^{red}.Zn^{2+}$ have been deposited in the Protein Data Bank (5frh and 5frf, respectively).

Data availability statement – Structure coordinates of $RsrA^{ox}$ and $RsrA^{red}.Zn^{2+}$ have been deposited in the Protein Data Bank (5frh and 5frf, respectively). NMR assignment data have been deposited at BMRB (accession numbers 25955 and 25956 for $RsrA^{red}.Zn^{2+}$ and $RsrA^{Ox}$ respectively).. All other relevant data are available from the authors on request.

References

1. Murphy, M.P. How mitochondria produce reactive oxygen species. *Biochem J* **417**, 1-13 (2009).
2. Malhotra, J.D. & Kaufman, R.J. Endoplasmic reticulum stress and oxidative stress: a vicious cycle or a double-edged sword? *Antioxid Redox Signal* **9**, 2277-93 (2007).
3. Storz, G. & Imlay, J.A. Oxidative stress. *Curr Opin Microbiol* **2**, 188-94 (1999).
4. Ye, Z.W., Zhang, J., Townsend, D.M. & Tew, K.D. Oxidative stress, redox regulation and diseases of cellular differentiation. *Biochim Biophys Acta* **1850**, 1607-21 (2015).
5. Carmel-Harel, O. & Storz, G. Roles of the glutathione- and thioredoxin-dependent reduction systems in the Escherichia coli and saccharomyces cerevisiae responses to oxidative stress. *Annu Rev Microbiol* **54**, 439-61 (2000).
6. Lu, J. & Holmgren, A. The thioredoxin antioxidant system. *Free Radic Biol Med* **66**, 75-87 (2014).
7. Green, J. & Paget, M.S. Bacterial redox sensors. *Nat Rev Microbiol* **2**, 954-66 (2004).
8. Paget, M.S. & Buttner, M.J. Thiol-based regulatory switches. *Annu Rev Genet* **37**, 91-121 (2003).
9. Imlay, J.A. Transcription Factors That Defend Bacteria Against Reactive Oxygen Species. *Annu Rev Microbiol* **69**, 93-108 (2015).
10. Paget, M.S., Kang, J.G., Roe, J.H. & Buttner, M.J. sigmaR, an RNA polymerase sigma factor that modulates expression of the thioredoxin system in response to oxidative stress in Streptomyces coelicolor A3(2). *EMBO J* **17**, 5776-82 (1998).
11. Kang, J.G. et al. RsrA, an anti-sigma factor regulated by redox change. *EMBO J* **18**, 4292-8 (1999).
12. Hughes, K.T. & Mathee, K. The anti-sigma factors. *Annu Rev Microbiol* **52**, 231-86 (1998).
13. Campbell, E.A. et al. A conserved structural module regulates transcriptional responses to diverse stress signals in bacteria. *Mol Cell* **27**, 793-805 (2007).
14. Newman, J.D., Falkowski, M.J., Schilke, B.A., Anthony, L.C. & Donohue, T.J. The Rhodobacter sphaeroides ECF sigma factor, sigma(E), and the target promoters cycA P3 and rpoE P1. *J Mol Biol* **294**, 307-20 (1999).
15. Helmann, J.D. Anti-sigma factors. *Curr Opin Microbiol* **2**, 135-41 (1999).
16. Kaushal, D. et al. Reduced immunopathology and mortality despite tissue persistence in a Mycobacterium tuberculosis mutant lacking alternative sigma factor, SigH. *Proc Natl Acad Sci U S A* **99**, 8330-5 (2002).
17. Kim, M.S. et al. Conservation of thiol-oxidative stress responses regulated by SigR orthologues in actinomycetes. *Mol Microbiol* **85**, 326-44 (2012).
18. Anthony, J.R., Warczak, K.L. & Donohue, T.J. A transcriptional response to singlet oxygen, a toxic byproduct of photosynthesis. *Proc Natl Acad Sci U S A* **102**, 6502-7 (2005).
19. Newman, J.D., Anthony, J.R. & Donohue, T.J. The importance of zinc-binding to the function of Rhodobacter sphaeroides ChrR as an anti-sigma factor. *J Mol Biol* **313**, 485-99 (2001).
20. Ziegelhoffer, E.C. & Donohue, T.J. Bacterial responses to photo-oxidative stress. *Nat Rev Microbiol* **7**, 856-63 (2009).
21. Cao, M., Wang, T., Ye, R. & Helmann, J.D. Antibiotics that inhibit cell wall biosynthesis induce expression of the Bacillus subtilis sigma(W) and sigma(M) regulons. *Mol Microbiol* **45**, 1267-76 (2002).
22. Thakur, K.G., Praveena, T. & Gopal, B. Structural and biochemical bases for the redox sensitivity of Mycobacterium tuberculosis RslA. *J Mol Biol* **397**, 1199-208 (2010).
23. Paget, M.S. et al. Mutational analysis of RsrA, a zinc-binding anti-sigma factor with a thiol-disulphide redox switch. *Mol Microbiol* **39**, 1036-47 (2001).

24. Zdanowski, K. et al. Assignment of the zinc ligands in RsrA, a redox-sensing ZAS protein from Streptomyces coelicolor. *Biochemistry* **45**, 8294-300 (2006).
25. Li, W. et al. The Role of zinc in the disulphide stress-regulated anti-sigma factor RsrA from Streptomyces coelicolor. *J Mol Biol* **333**, 461-72 (2003).
26. Bae, J.B., Park, J.H., Hahn, M.Y., Kim, M.S. & Roe, J.H. Redox-dependent changes in RsrA, an anti-sigma factor in Streptomyces coelicolor: zinc release and disulfide bond formation. *J Mol Biol* **335**, 425-35 (2004).
27. Sevier, C.S. & Kaiser, C.A. Formation and transfer of disulphide bonds in living cells. *Nat Rev Mol Cell Biol* **3**, 836-47 (2002).
28. Wei, Z.H., Chen, H., Zhang, C. & Ye, B.C. FRET-based system for probing protein-protein interactions between sigmaR and RsrA from Streptomyces coelicolor in response to the redox environment. *PLoS One* **9**, e92330 (2014).
29. Owen, G., Pascoe, B., Kallifidas, D. & Paget, M. - Zinc-responsive regulation of alternative ribosomal protein genes in Streptomyces. *J Bacteriol* **189**, 4078-86 (2007).
30. Kosower, N.S. & Kosower, E.M. Diamide: an oxidant probe for thiols. *Methods Enzymol* **251**, 123-33 (1995).
31. Heo, L., Cho, Y.B., Lee, M.S., Roe, J.H. & Seok, C. Alternative zinc-binding sites explain the redox sensitivity of zinc-containing anti-sigma factors. *Proteins* **81**, 1644-52 (2013).
32. Traore, D.A. et al. Structural and functional characterization of 2-oxo-histidine in oxidized PerR protein. *Nat Chem Biol* **5**, 53-9 (2009).
33. Jakob, U., Muse, W., Eser, M. & Bardwell, J.C. Chaperone activity with a redox switch. *Cell* **96**, 341-52 (1999).
34. Choi, H. et al. Structural basis of the redox switch in the OxyR transcription factor. *Cell* **105**, 103-13 (2001).
35. Newberry, K.J., Fuangthong, M., Panmanee, W., Mongkolsuk, S. & Brennan, R.G. Structural mechanism of organic hydroperoxide induction of the transcription regulator OhrR. *Mol Cell* **28**, 652-64 (2007).
36. Lee, C. et al. Redox regulation of OxyR requires specific disulfide bond formation involving a rapid kinetic reaction path. *Nat Struct Mol Biol* **11**, 1179-85 (2004).
37. Fuangthong, M. & Helmann, J.D. The OhrR repressor senses organic hydroperoxides by reversible formation of a cysteine-sulfenic acid derivative. *Proc Natl Acad Sci U S A* **99**, 6690-5 (2002).
38. Ilbert, M. et al. The redox-switch domain of Hsp33 functions as dual stress sensor. *Nat Struct Mol Biol* **14**, 556-63 (2007).
39. Aslund, F., Zheng, M., Beckwith, J. & Storz, G. Regulation of the OxyR transcription factor by hydrogen peroxide and the cellular thiol-disulfide status. *Proc Natl Acad Sci U S A* **96**, 6161-5 (1999).
40. Heinrich, J., Hein, K. & Wiegert, T. Two proteolytic modules are involved in regulated intramembrane proteolysis of Bacillus subtilis RsiW. *Mol Microbiol* **74**, 1412-26 (2009).
41. Li, W. et al. Identification and structure of the anti-sigma factor-binding domain of the disulphide-stress regulated sigma factor sigma(R) from Streptomyces coelicolor. *J Mol Biol* **323**, 225-36 (2002).
42. Sobott, F., Hernandez, H., McCammon, M.G., Tito, M.A. & Robinson, C.V. A tandem mass spectrometer for improved transmission and analysis of large macromolecular assemblies. *Anal Chem* **74**, 1402-7 (2002).
43. Hernandez, H. & Robinson, C.V. Determining the stoichiometry and interactions of macromolecular assemblies from mass spectrometry. *Nat Protoc* **2**, 715-26 (2007).
44. Rose, R.J., Damoc, E., Denisov, E., Makarov, A. & Heck, A.J. High-sensitivity Orbitrap mass analysis of intact macromolecular assemblies. *Nat Methods* **9**, 1084-6 (2012).
45. Dyachenko, A. et al. Tandem Native Mass-Spectrometry on Antibody-Drug Conjugates and Submillion Da Antibody-Antigen Protein Assemblies on an Orbitrap

EMR Equipped with a High-Mass Quadrupole Mass Selector. *Anal Chem* **87**, 6095-102 (2015).
46. Lakowicz, J.R. *Principles of Fluorescence Spectroscopy*, (Springer, 2006).
47. Hunt, J.B., Neece, S.H. & Ginsburg, A. The use of 4-(2-pyridylazo)resorcinol in studies of zinc release from Escherichia coli aspartate transcarbamoylase. *Anal Biochem* **146**, 150-7 (1985).
48. Rost, J. & Rapoport, S. REDUCTION-POTENTIAL OF GLUTATHIONE. *Nature* **201**, 185 (1964).
49. Sigurskjold, B.W. Exact analysis of competition ligand binding by displacement isothermal titration calorimetry. *Anal Biochem* **277**, 260-6 (2000).
50. Marino, F. et al. Characterization and usage of the EASY-spray technology as part of an online 2D SCX-RP ultra-high pressure system. *Analyst* **139**, 6520-8 (2014).
51. Chambers, M.C. et al. A cross-platform toolkit for mass spectrometry and proteomics. *Nat Biotechnol* **30**, 918-20 (2012).
52. Yang, B. et al. Identification of cross-linked peptides from complex samples. *Nat Methods* **9**, 904-6 (2012).
53. Campbell, E.A. et al. Crystal structure of Escherichia coli sigmaE with the cytoplasmic domain of its anti-sigma RseA. *Mol Cell* **11**, 1067-78 (2003).
54. Sali, A. & Blundell, T.L. Comparative protein modelling by satisfaction of spatial restraints. *J Mol Biol* **234**, 779-815 (1993).
55. Delaglio, F., Grzesiek, S., Vuister, G.W., Zhu, G., Pfeifer, J. and Bax, A. NMRPipe: a multidimensional spectral processing system based on UNIX pipes. *J. Biomol. NMR* **6**, 277-293 (1995).
56. Vranken, W.F., Boucher, W., Stevens, T.J., Fogh, R.H., Pajon, A., Llinas, M., Ulrich, E.L., Markley, J.L., Ionides, J. and Laue, E.D. The CCPN data model for NMR spectroscopy: Development of a software pipeline. *Proteins: Structure, Function, and Bioinformatics* **59**, 687-696 (2005).
57. Tjandra, N. & Bax, A. Direct measurement of distances and angles in biomolecules by NMR in a dilute liquid crystalline medium. *Science* **278**, 1111-4 (1997).
58. Ottiger, M., Delaglio, F. & Bax, A. Measurement of J and dipolar couplings from simplified two-dimensional NMR spectra. *J Magn Reson* **131**, 373-378 (1998).
59. Rückert, M. & Otting, G. Alignment of biological macromolecules in novel nonionic liquid crystalline media for NMR experiments. *J Am Chem Soc* **122**, 7793-7797 (2000).
60. Goddard, T.D. & Kneller, D.G. SPARKY 3. *University of California, San Francisco*.
61. Dosset, P., Hus, J.C., Marion, D. & Blackledge, M. A novel interactive tool for rigid-body modeling of multi-domain macromolecules using residual dipolar coupling. *J Biomol NMR* **20**, 223-231 (2001).
62. Brunger AT et al. Crystallography & NMR system: A new software suite for macromolecular structure determination. *Acta Crystallogr D Biol Crystallogr.* **54**, 905-921 (1998).
63. Rudino-Pinera, E. et al. The Solution and Crystal Structures of a Module Pair from the Staphylococcus aureus-Binding Site of Human Fibronectin--A Tale with a Twist. *J Mol Biol* **368**, 833-844 (2007).
64. Cornilescu, G., Delaglio, F. & Bax, A. Protein backbone angle restraints from searching a database for chemical shift and sequence homology. *J Biomol NMR* **13**, 289-302 (1999).
65. Vriend, G. WHAT IF: a molecular modeling and drug design program. *J Mol Graph* **8**, 52-56 (1990).
66. Kim, M.S., Hahn, M.Y., Cho, Y., Cho, S.N. & Roe, J.H. Positive and negative feedback regulatory loops of thiol-oxidative stress response mediated by an unstable isoform of sigmaR in actinomycetes. *Mol Microbiol* **73**, 815-25 (2009).

Acknowledgements

We thank Nick Housden and Grigorios Papadakos (Department of Biochemistry, Oxford) for guidance on the kinetic and thermodynamic measurements in this paper. We are indebted to Mark Buttner and Morgan Feeney (John Innes Centre, Norwich) for comments on the manuscript and Joseph Gault (Department of Chemistry, Oxford) for help acquiring high-resolution MS data. This work was funded by BBSRC grant BB/I008691/1. JRP holds a British Heart Foundation Senior Basic Science Fellowship (FS/12/36/29588), JMW and LP would like to thank the Wellcome Trust for support of the Southampton NMR centre (grant No: 090658/Z/09/Z) and the MRC for support of the Biomedical NMR Centre at Mill Hill (grant No. U117533887).

Author contributions

K.V.R. conducted the kinetic, thermodynamic and oxidation experiments, modelled the complex and prepared mutants and cross-linked samples. K.Z., L.P., J.M.W. & J.R.P. determined NMR structures of RsrA. J.Y., J.T.S.H., S.M. & C.V.R. conducted the mass spectrometry experiments and associated analysis. M.L.F. contributed to kinetic analysis and with C.Se. prepared samples. C.Sh. & K.V.R. conducted the bioinformatics analysis. C.K. was the principal investigator and, along with K.V.R., prepared the manuscript.

Competing financial interests

The authors declare no competing financial interests.

Figure Legends

Figure 1. Scheme showing redox homeostasis loop for the RsrA-σ^R complex. The figure highlights the zinc coordination residues in reduced RsrA ($RsrA^{red}.Zn^{2+}$) from *Streptomyces coelicolor*. Disulfide stress results in the loss of zinc and formation of a degenerate trigger disulfide bond in $RsrA^{ox}$, formed by the same zinc-binding residues. The transcribed regulon of σ^R includes anti-oxidant genes that re-establish redox homeostasis and the genes for *sigR* and *rsrA* (not shown), which amplify the response. Not shown is an additional layer of regulation involving a form of σ^R with an N-terminal extension that also binds RsrA but is rapidly degraded by proteolysis[66]. Shaded panels denote NMR structures of RsrA reported in the present work.

Figure 2. Redox potential of the $RsrA^{red}.Zn^{2+}$-σ^R complex. ***a***, $RsrA^{red}.Zn^{2+}$ binding to σ^R monitored by intrinsic tryptophan emission fluorescence spectroscopy. Figure shows emission spectra (λ_{ex} 295 nm) of σ^R at different $RsrA^{red}.Zn^{2+}$ concentrations collected at 25˚C in 50 mM Tris pH 7.5 buffer, 100 mM NaCl, 2 mM DTT. For clarity, traces are coloured with incrementally darker tone of grey for increasing RsrA concentration. Inset figure shows fraction of σ^R in complex as measured by the change in fluorescence intensity at 343 nm with increasing $RsrA^{red}.Zn^{2+}$ concentration. Data show stoichiometric binding of $RsrA^{red}.Zn^{2+}$ to σ^R. ***b***, Redox potential of $RsrA^{red}.Zn^{2+}$ in complex with σ^R complex relative to a redox couple of reduced/oxidized glutathione. The degree of oxidation was measured by the change in tryptophan emission fluorescence of σ^R as the complex dissociates (*open triangles*) and by the release of Zn^{2+} using the PAR assay (*filled triangles*). Both sets of data were fitted to the Nernst equation to determine the redox potential of the $RsrA^{red}$-Zn^{2+}-σ^R complex as -193.04 ± 2.01 mV. Experiments were conducted in 50 mM Tris pH 7.5 buffer containing 100 mM NaCl and at 25˚C. ***c***, Redox ruler showing the redox potentials of

selected proteins and small molecules. Figure adapted from[27]. The estimated redox potential of the bacterial cytoplasm is indicated in grey.

Figure 3. Zinc slows the dissociation rate of the high affinity RsrA^{red}.Zn^{2+}-σ^{R} complex. Conditions used for all experiments were 50 mM Tris pH 7.5 buffer containing 100 mM NaCl and 2 mM DTT. Temperature was either 35°C (panels a and b) or 25°C (panels c and d). ***a***, Competition ITC data for RsrA^{red}.Zn^{2+} (100 μM) binding σ^{R} (10 μM, cell concentration) in the presence of RsrA* Cys11Ser Cys44Ser (50 μM). RsrA* Cys11Ser Cys44Ser binds σ^{R} with a weaker affinity than wild type RsrA (**Supplementary Table 1**). Control data show titration of RsrA^{red}.Zn^{2+} into buffer containing 50 μM RsrA* Cys11Ser Cys44Ser. Fitted parameters for a competitive binding site model from three independent measurements were N = 1.01 ± 0.05, K_d = 0.78 ± 0.034 nM, ΔH = -23.05 ± 1.10 kcal/mol, ΔS= -38.70 ± 3.10 cal/mol/deg. ***b***, Direct ITC data for RsrA^{red} (100 μM) binding σ^{R} (10 μM) in the absence of zinc. Control data show titration of RsrA^{red} into buffer. Fitted parameters for a single site binding model were N = 0.97 ± 0.004, K_d = 79.3 ± 4.2 nM, ΔH = -16.26 ± 0.13 kcal/mol, ΔS = -20.3 ± 4.34 cal/mol/deg. ***c***, *Main panel*, tryptophan emission fluorescence stopped-flow association data for RsrA^{red}.Zn^{2+} binding σ^{R} under pseudo-first order conditions (λ_{ex}, 295 nm). Residuals to the fit of a single exponential are shown below the panel. *Inset*, pseudo-first order plot of observed rates (k_{obs}) as a function of RsrA concentration in the presence and absence of stoichiometric zinc (with associated error bars). See **Supplementary Table 2** for derived values of k_{on}. Error bars are within the data point symbols. ***d***, Dissociation of the RsrA^{red}-σ^{R} complex measured by competition stopped-flow in which a 10-fold excess of σ^{R} Trp88Ile Trp119Ile was used to displace wild-type σ^{R} (see Materials and Methods). Main panel shows data for the RsrA^{red}-σ^{R} complex in the absence of bound zinc. *Inset*, dissociation data for the RsrA^{red}-σ^{R} complex in the presence of one and three equivalents of zinc (*open* and *filled triangles*, respectively). See **Supplementary Table 2** for values of k_{off}.

Figure 4. Zinc release is the rate-limiting step in RsrA oxidation. Experiments were conducted at 25˚C in 50 mM Tris pH 7.5 buffer containing 100 mM NaCl. ***a***, Oxidation of the RsrA-σ^R complex on treatment with diamide under second-order conditions (25 μM). The fraction of reduced RsrA was determined by the change in diamide absorbance at 320 nm (**Supplementary Figure 2a**) in the presence and absence of bound zinc. Zinc release was monitored at 500 nm using the PAR assay. The two methods showed good agreement for the bimolecular rate constant for diamide-induced oxidation of $RsrA^{red}.Zn^{2+}$ (183 ± 6 $M^{-1}s^{-1}$ and 195 ± 11 $M^{-1}s^{-1}$, respectively). ***b***, Zinc release from the $RsrA^{red}.Zn^{2+}$-σ^R complex (2 μM) on treatment with increasing concentrations of diamide under pseudo-first-order conditions monitored by the PAR assay; 25 μM (*filled diamonds*), 50 μM, 100 μM, 150 μM and 200 μM (*open diamonds*). Inset shows variation of k_{obs} with diamide concentration (with associated error bars). Data were fitted to the Michealis-Menten equation, with fitted parameters of K_1 = 0.7 mM and k_2 = 0.15 s^{-1} (See **Supplementary Figure 2b**). The corresponding bimolecular rate constant (k_2/K_1 = 214 $M^{-1}s^{-1}$) is in reasonable agreement with values obtained in *a*. ***c***, Oxidation-induced dissociation of the $RsrA^{red}.Zn^{2+}$-σ^R complex (2 μM) monitored by tryptophan fluorescence on treatment with H_2O_2 under pseudo-first order conditions. Three H_2O_2 concentrations are shown; 1 mM (*triangles*), 2 mM (*open circles*) and 6 mM (*closed circles*). *Inset*, pseudo-first order plot (with associated error bars) from which the bimolecular rate constant for H_2O_2 induced dissociation of the complex was obtained (0.39 ± 0.08 M^{-1} s^{-1}). ***d***, Zinc release from the $RsrA^{red}.Zn^{2+}$-σ^R complex (2 μM) on treatment with increasing concentrations of H_2O_2 (2-10 mM) under pseudo-first order conditions. *Inset*, pseudo-first order plot (with associated error bars) from which the bimolecular rate constant for the H_2O_2-induced zinc dissociation was obtained (0.32 ± 0.06 M^{-1} s^{-1}).

Figure 5. Cys11 is essential for redox sensing in RsrA. Zinc ligation for each RsrA construct used is shown as a schematic. ***a***, Comparing the intrinsic dissociation rates of σ^R complexes with $RsrA^{*red}.Zn^{2+}$ (*open triangles*; k_{off} = 0.0027 s^{-1}) and $RsrA^{*red}.Zn^{2+}$ Cys11His (*closed triangles*; k_{off} = 0.064 s^{-1}) obtained by competition stopped-flow tryptophan emission

fluorescence using a 10-fold excess of σ^R Trp88Ile Trp119Ile. All experiments were conducted at 25˚C in 50 mM Tris pH 7.5 buffer containing 100 mM NaCl. *Inset*, dissociation data in the presence (*closed circles*) and absence (*open circles*) of zinc for σ^R in complex with triple mutant RsrA* Cys11His Cys41His Cys44His (k_{off} ~ 2.3 s^{-1}). ***b***, Comparison of H_2O_2 (10 mM) induced dissociation of the RsrA*^{red}.Zn^{2+}-σ^R complex (*closed circles*) with RsrA*^{red}.Zn^{2+} Cys11His-σ^R (*open circles*) and RsrA*^{red}.Zn^{2+} Cys11His Cys41His Cys44His (*closed triangles*) complexes. Data for complexes of RsrA* Cys41His and RsrA* Cys44His, shown in **Supplementary Figure 4**, were essentially identical to RsrA*. The absence of Cys11 renders RsrA insensitive to oxidation-induced dissociation from its complex with σ^R. ***c***, *Upper panel*, native state mass spectrometry data for RsrA*^{red}.Zn^{2+} Cys11His in complex with σ^R showing the predominance of the zinc-bound species (theoretical/observed mass, 40,128.08/40,127.54 ± 0.12 Da, respectively). The minor species was the reduced complex without zinc bound (theoretical /observed mass, 40,064.72/40,064.41 ± 0.66 Da, respectively). *Lower panel*, the same complex following treatment with 10 mM H_2O_2. Although RsrA* Cys11His remains in complex with σ^R the metal ion has dissociated and the remaining cysteines (Cys41 and Cys44) have formed a disulfide bond, as deduced by the ~2 Da reduction in mass (theoretical/observed mass, 40,062.70/40,061.96 ± 0.28 Da, respectively).

Figure 6. Solution structures of RsrA^{red}.Zn^{2+} and RsrA^{ox}. ***a***, Comparison of ^1H-^{15}N HSQC spectra of reduced RsrA* Cys41Ser (RsrA^{red}-Zn^{2+}, *blue peaks*), in 20 mM Tris buffer pH 7.1 containing 5 mM DTT and 2 mM $ZnCl_2$, with RsrA^{ox} (*red peaks*), which is the same protein in the same buffer but in the absence of reductant and metal ions. ***b***, Overlay of the 10 lowest energy structures for RsrA^{red}-Zn^{2+} (residues Glu8-Gln86; left-hand figure) and a ribbon diagram of the lowest energy structure (right-hand figure), showing the location of the zinc-binding residues (His37, blue; Cys41Ser, cyan; Cys11 and Cys44, yellow) and the zinc atom (blue). ***c***, Overlay of the 10 lowest energy structures for RsrA^{ox} (residues Glu8-Gln86; left-hand figure) and a ribbon diagram of the lowest energy structure (right-hand figure),

showing the location of the disulfide bond and disruption of the metal site following oxidation (residues and helices are coloured as in *b*).

Figure 7. $RsrA^{red}.Zn^{2+}$ uses hydrophobic core residues to bind σ^R that are sequestered to the $RsrA^{ox}$ interior following oxidation. ***a***, Solution structure of $RsrA^{red}.Zn^{2+}$. RsrA helices are coloured N-to-C as in the sequence alignment in panel d. Zinc is shown as a blue sphere and zinc ligands coloured by atom type. Conserved or conservatively substituted hydrophobic residues that contribute to RsrA's hydrophobic core in all three of its structural states (*a-c*) are coloured green while those that also interact with σ^R are coloured red. ***b***, Homology model of the $RsrA^{red}.Zn^{2+}$-σ^R complex validated by homo-bifunctional lysine-specific cross-linking (see **Supplementary Figure 4**). The structure of $RsrA^{red}.Zn^{2+}$ changes dramatically to embrace σ^R. ***c***, Solution structure of $RsrA^{ox}$ where the trigger disulfide is formed between residues Cys11 and Cys44, expelling bound zinc and repacking the hydrophobic core. ***d***, Sequence alignment of RsrA and other ZAS proteins (ChrR, RshA and RslA). Zinc ligands in each protein are underlined. Helices in all three structural forms of RsrA are coloured as in panels *a-c*. Vertical green shading shows conserved hydrophobic residues that contribute to the hydrophobic core of RsrA in all three structural states ($RsrA^{red}.Zn^{2+}$, $RsrA^{red}.Zn^{2+}$-σ^R complex and $RsrA^{ox}$). Vertical red shading shows conserved hydrophobic residues in RsrA that contribute to the hydrophobic cores of $RsrA^{red}.Zn^{2+}$ and $RsrA^{ox}$ but also contribute to the protein-protein interface in the $RsrA^{red}.Zn^{2+}$-σ^R complex.

Supplementary figure legends

Supplementary Figure 1. Zinc binding to RsrA. ***a***, Far-UV CD spectra of RsrA* incubated with increasing concentrations of zinc (in 10 mM Tris pH 7.5, at 20˚C) starting from apo-protein (*blue spectrum*). Wild type RsrA yielded poor CD spectra and so zinc titrations were performed with RsrA*. The protein becomes more helical as the amount of zinc increases but saturates at one equivalent of zinc (*red spectrum*). ***b***, Figure shows variation of RsrA* mdeg at 222 nm starting from apo-RsrA* (*blue square*, equivalent to blue spectrum in *b*) with increasing zinc concentration. *Red square* is equivalent to the red spectrum in *b*. ***c***, Native-state ESI-MS spectrum of apo-RsrA* (same sample used in CD experiment, blue point in *c*). ***d***, Native-state ESI-MS spectrum of RsrA* incubated with 1 equivalent of zinc (same sample used in CD experiment, red point in *c*). Protein was buffer exchanged into 20 mM ammonium acetate before data collection (theoretical/observed masses for apo- and single zinc bound to RsrA* are 11834/11832.82 ± 0.57 and 11897/11896.75 ± 1.02, respectively). **. *e***, Stoichiometry of zinc binding to wild type RsrA. Figure shows the high resolution native-state ESI-MS spectrum of RsrA incubated with excess zinc. 10 µM RsrA was dissolved in 50 mM Tris HCl pH 7.5, 100 mM NaCl, 0.1 mM $ZnCl_2$ and 10 mM DTT. Samples were buffer exchanged into 20 mM ammonium acetate before measurements were made. Spectrum shows up to 3 Zn^{2+} ions bind to RsrA. Theoretical and observed masses for apo, $1Zn^{2+}$, $2Zn^{2+}$ and $3Zn^{2+}$ bound samples were 11962.3/11957.08 ± 4.90 Da, 12025.3/12022.72 ± 6.21 Da, 12088.3/12087.36 ± 5.36 Da and 12151.3/12154.20 ± 4.46 Da respectively. Similar data were obtained for RsrA*, where all non-essential cysteines (Cys3, Cys31, Cys61 and Cys62) were mutated to alanine, indicating that non-stoichiometric zinc binding is not associated with cysteine residues outside of the ZAS sequence motif.

Supplementary Figure 2. Diamide oxidation kinetics. ***a*****,** Schematic showing the chemical conversion of diamide from the diazene to hydrazine forms during the oxidation of RsrA. Also shown is the sulfenyl hydrazine intermediate. Spectroscopic measurement of diamide reduction by RsrA exploited the absorption of diamide at 320nm. The product hydrazine does not absorb at this wavelength. ***b*****,** Kinetic mechanism for diamide-induced oxidation of $RsrA^{red}.Zn^{2+}$. The mechanism is based on data obtained from diamide reduction kinetics (main text, **Figure 4b**). Values for K_1 and k_2 obtained from the data shown in Figure 5b were 0.7 mM and 0.15 s^{-1}, respectively. ***c***, Kinetics of $RsrA^{red}.Zn^{2+}$ oxidation by diamide are the same as for the $RsrA^{red}.Zn^{2+}$-σ^R complex. Experiments were conducted at 25˚C in 50 mM Tris HCl pH 7.5 buffer containing 100 mM NaCl. Proteins were first reduced with DTT (10 mM) then buffer exchanged to remove the reducing agent. Where indicated, stoichiometric zinc was added. Oxidation of and zinc release from $RsrA^{red}.Zn^{2+}$ on treatment with diamide under second-order conditions (25 μM) was measured spectrophotometrically (see Materials and Methods for further details). The fraction of reduced $RsrA^{red}.Zn^{2+}$ was determined by monitoring the change in diamide absorbance at 320 nm in the presence and absence of stoichiometric zinc (*open and closed circles*, respectively). Zinc release (*open squares*) was monitored at 500 nm using the PAR assay. For clarity, only every 80^{th} data point is shown in these curves. The two methods showed good agreement for the bimolecular rate constant for diamide-induced oxidation of $RsrA^{red}.Zn^{2+}$ (196 ± 12.3 M^{-1} $s^{-1}$and 194 ± 29 M^{-1} s^{-1}, respectively). Oxidation of RsrA was five-fold faster in the absence of zinc (946 ± 24 M^{-1} s^{-1}). These data closely mirror those obtained for RsrA bound to σ^R indicating that complex formation does not influence redox sensing by RsrA.

Supplementary Figure 3. Additional Zn^{2+} ions do not affect the rate of RsrA oxidation. ***a***, Competition ITC data for σ^R Trp88Ile Trp119Ile binding $RsrA^{red}.Zn^{2+}$, as described for the wild type complex (main text, **Figure 3a**). Fitted parameters for a single binding site model were N = 1.17 ± 0.09, K_d = 0.173 ± 0.034 nM, ΔH = -20.34 ± 0.91 kcal/mol**.** ***b***, Tryptophan

emission fluorescence spectroscopy was used to determine the kinetics of $RsrA^{red}$-σ^R oxidative dissociation on treatment with 10 mM H_2O_2 and increasing zinc stoichiometry. Oxidation induced dissociation of the $RsrA^{red}$-σ^R complex was the same regardless of whether 1 (*open circles*), 2 (*closed triangles*) or 3 (*closed circles*) equivalents of zinc, respectively, were added to the protein. ***c***, The rate of Zn^{2+} release from the $RsrA^{red}.Zn^{2+}$-σ^R complex on treatment with 15 mM diamide is the same when RsrA is bound with 1 (*diamonds*), 2 (*circles*) or 3 (*squares*) equivalents of zinc, respectively. Hence, increasing zinc stoichiometry does not influence redox sensing by the $RsrA^{red}.Zn^{2+}$-σ^R complex. *d*, Kinetic scheme of RsrA-σ^R interaction. ***d***, Kinetic scheme showing RsrA-σ^R protein-protein interactions and the influence of zinc and oxidant. Rate constants are taken from Figures 4 and 5. The kinetics of $RsrA^{red}.Zn^{2+}$-σ^R oxidation are those for a disulfide-containing oxidant, denoted by S-S in the scheme and mimicked by diamide in our experiments, to form a mixed disulfide ($RsrA^{-S}$), which we infer (Figure 4b). The oxidation process is a two-step reaction involving the slow loss of zinc followed by a fast step involving dissociation of σ^R and formation of the trigger disulfide bond (Cys11-Cys44 or Cys11-Cys41).

Supplementary Figure 4. **H_2O_2-induced dissociation of RsrA histidine mutants confirms the redundancy of the trigger disulfide bond**. Comparison of H_2O_2 (10 mM) induced dissociation of $RsrA^{*red}.Zn^{2+}$-σ^R complex (*open circles*) with $RsrA^{*red}.Zn^{2+}$ Cys11His-σ^R (*closed circles*), $RsrA^{*red}.Zn^{2+}$ Cys41His-σ^R (*closed triangles*) and $RsrA^{*red}.Zn^{2+}$ Cys44His-σ^R (*open triangles*) complexes. The data emphasise the redundancy of the trigger disulfide bond in RsrA in which either Cys41 or Cys44 can form a disulfide with Cys11 to release σ^R.

Supplementary Figure 5. Cross-linking based homology model of the $RsrA^{red}.Zn^{2+}$-σ^R complex. ***a,*** The $RsrA^{red}.Zn^{2+}$-σ^R complex (RsrA, blue; σ^R σ^2 domain, orange, and σ^4 domain, pink) was modelled on three anti-sigma factor-sigma factor complexes, *E. coli*

RseA-σ^E (sequence identity 15.8%, pdb code 1OR7), *R. sphaeroides* ChrR-RpoE/σ^E (sequence identity 11.1%, pdb code 2Q1Z) and *M. tuberculosis* RslA-σ^L (sequence identity 20.6%, pdb code 3HUG). Only ChrR and RslA are ZAS proteins but all three have the so-called ASD fold. The structure of the RslA-σ^L complex only contains half of the sigma factor (σ^4 domain) whereas the other complexes have both σ^2 and σ^4 domains. Red lines indicate the lysine-specific crosslinks observed for the RsrA^{red}.Zn^{2+}-σ^R complex mapped onto each model. The table beneath the structures shows the solvent accessible surface distances for lysines in the RsrA^{red}.Zn^{2+}-σ^R complex predicted for the different models and summarizes the cross-links observed for the different homo-bifunctional cross-linkers used (BS3, bis(sulfosuccinimidyl)suberate, 11.4 Å cross-linking distance; BS2G, bis(sulfosuccinimidyl) 2,2,4,4-glutarate), 7.7 Å cross-linking distance. NK, not known. The cross-links observed in the RsrA^{red}.Zn^{2+}-σ^R complex (*left hand panel*) indicated the complex was most similar to the ChrR-RpoE complex but also had similarities to the RslA-σ^L complex. ***b***, Strategy used to obtain lysine-specific cross-linking data for the RsrA^{red}.Zn^{2+}-σ^R complex. RsrA^{red}.Zn^{2+}-σ^R complex was incubated with a 2 mM mixture of BS^2G-d_0 and BS^2G-d_4 in 20 mM Hepes pH 7.5, 50 mM NaCl and 2 mM DTT at room temperature for 30 minutes. Cross-linking was stopped with 100 mM Tris pH 7.5. Samples were run on an SDS-PAGE and protein bands excised and analysed by LC-MS/MS. (Crosslinking with BS3-d_0/BS3-d_4 was done similarly). Crosslinks to all residues except RsrA K74 are coloured red. Crosslinks to RsrA K74 to σ^R K71 is coloured yellow, RsrA K74 to σ^R K86 is coloured black and RsrA K74 to σ^R K149 is coloured blue. A single unique intramolecular cross-link within RsrA (56K-74K) was observed (XLR in the gel) which agrees with the solution structure of RsrA^{red}.Zn^{2+}. ***c***, Homology model of the RsrA^{red}.Zn^{2+}-σ^R complex showing two possible conformations of helix IV. Model was built based on homology with ChrR-RpoE and RslA-σ^L using Modeller V9.12. 100 models were generated and the lowest energy model shown. RsrA is coloured blue, σ^2 domain of σ^R is coloured orange, σ^4 domain of σ^R is coloured pink. Cylinders denote helices and are coloured as in *a*. Red lines denote the observed crosslinks. RsrA keeps the same

fold in both the models except for the orientation of the final helix which could interact with either σ^2 or σ^4.

Supplementary Figure 6. ^{1}H-^{15}N HSQC spectra of reduced and oxidized RsrA. ***a***, ^{1}H-^{15}N-HSQC spectrum of RsrA*^{red} Cys41Ser in the absence of zinc (black) and bound to one equivalent of zinc (blue) in 20 mM Tris buffer pH 7.1 containing 5 mM DTT and 2 mM $ZnCl_2$, with RsrA^{Ox} (red peaks) in the same buffer but in the absence of reductant and metal ions. ***b***, Oxidised RsrA proteins containing either Cys11-Cys41 or Cys11-Cys44 disulfide bonds yield well-dispersed HSQC spectra characteristic of globular, folded proteins. Overlay of HSQC spectra of oxidized RsrA* Cys44Ser containing the Cys11-Cys41 disulfide bond (*black peaks*) and RsrA* Cys41Ser containing the Cys11-Cys44 disulfide bond (*red peaks*).

Supplementary Figure 7. Identification of the most stable trigger disulfide bond in RsrA^{ox}. ***a***, Schematic of RsrA showing the location of cysteine residues mutated to alanine in RsrA*, the identity of the zinc ligands and the trigger disulfide bond that forms in response to oxidation and which results in the loss of zinc. Previous studies have shown that the trigger disulfide is degenerate and forms between either Cys11 and Cys41 or Cys11 and Cys44. ***b***, Time-dependent changes in far UV-CD spectra (0.16 mg/ml) during formation of the RsrA* Cys11-Cys44 disulfide bond in RsrA* C41S as a result of air oxidation in 20 mM Tris pH 7.1, 25°C are similar to those previously reported for wild-type RsrA [25]. ***c***, Overlay of ^{1}H-^{15}N-HSQC spectra of air-oxidized RsrA* (*blue peaks*), from which zinc had been removed, with ^{1}H-^{15}N-HSQC spectra of RsrA*^{ox} containing either the Cys11-Cys41 disulfide bond (*black peaks*) or the Cys11-Cys44 disulfide bond (*red peaks*). In each of the pure disulfided species of RsrA the third cysteine was mutated to serine to block mixed disulfide bond formation. The figure shows a comparison of three chemical shift regions demonstrating the overall similarity of the spectra of RsrA*^{ox} with RsrA*^{ox} containing the

Cys11-Cys44 disulfide bond (lower panels in the three spectral regions shown) rather than the Cys11-Cys41 disulfide bond. Assignments for glycine residues in RsrA*^{ox} Cys11-Cys44 are shown.

Supplementary Figure 8. Comparison of the ZAS and ASD folds. ***a***, Structural alignment of RsrA^{red}-Zn^{2+}(ZAS fold coloured *red*) and RsrA^{red}-Zn^{2+} in complex with σ^R (ASD fold coloured *green*). Helices are numbered from I to IV. Zinc is shown as a *blue sphere*, zinc ligands are shown as sticks and coloured based on atom type. Hydrophobic residues that form RsrA's core in both RsrA^{red}-Zn^{2+} and the RsrA^{red}-Zn^{2+}-σ^R complex are shown as *green sticks*. Hydrophobic residues that form RsrA's core in RsrA^{red}-Zn^{2+} but also form interactions with the sigma factor in the RsrA^{red}-Zn^{2+}-σ^R complex are shown as *red sticks*. The figure highlights how the ASD and ZAS folds represent different structural states of the same anti-sigma factor. ***b***, Structure-based sequence alignment of distantly related ZAS proteins from different phyla. *Streptomyces* and *Mycobacterium* belong to actinobacteria, *Clostirudium* belongs to Firmicutes, *Rhodopirellula* under Planctomycetes, *Treponema* under Spirochaetes , *Cytophaga* under Bacteroidetes, *Chloroherpeto* under Chlorobi, *Roseiflexus* under Chloroflexi, *Zantobacter, thioflavicoccus and Myxococcus* under Proteobacteria. Helix limits of RsrA$^{red.}$$Zn^{2+}$ and RsrA^{red}Zn^{2+}-σ^R complex are shown by *blue* and *green* horizontal bars, respectively. Hydrophobic residues are coloured as in *a*. Conserved hydrophobic residues in helices I and II (*green*) are involved primarily in stabilizing both the ZAS and ASD folds. In contrast, conserved hydrophobic residues in helices III and IV (*red*) have a dual role, stabilizing the ZAS fold in the absence of sigma factor and the protein-protein interaction with sigma factor. ***c***, Abundance of ZAS-ECF complexes in bacteria. The figure shows all organisms that have a ZAS domain close to an ECF. Searching for proteins similar to RsrA or ChrR with a zinc motif (C/H-x(23-26)-H-x(3)-C-x(2)-C) that lie less than 300 bases away from an ECF-σ homolog showed that more than 1100 genomes have ECF-ZAS pairs. Different sector colours denote different phyla.

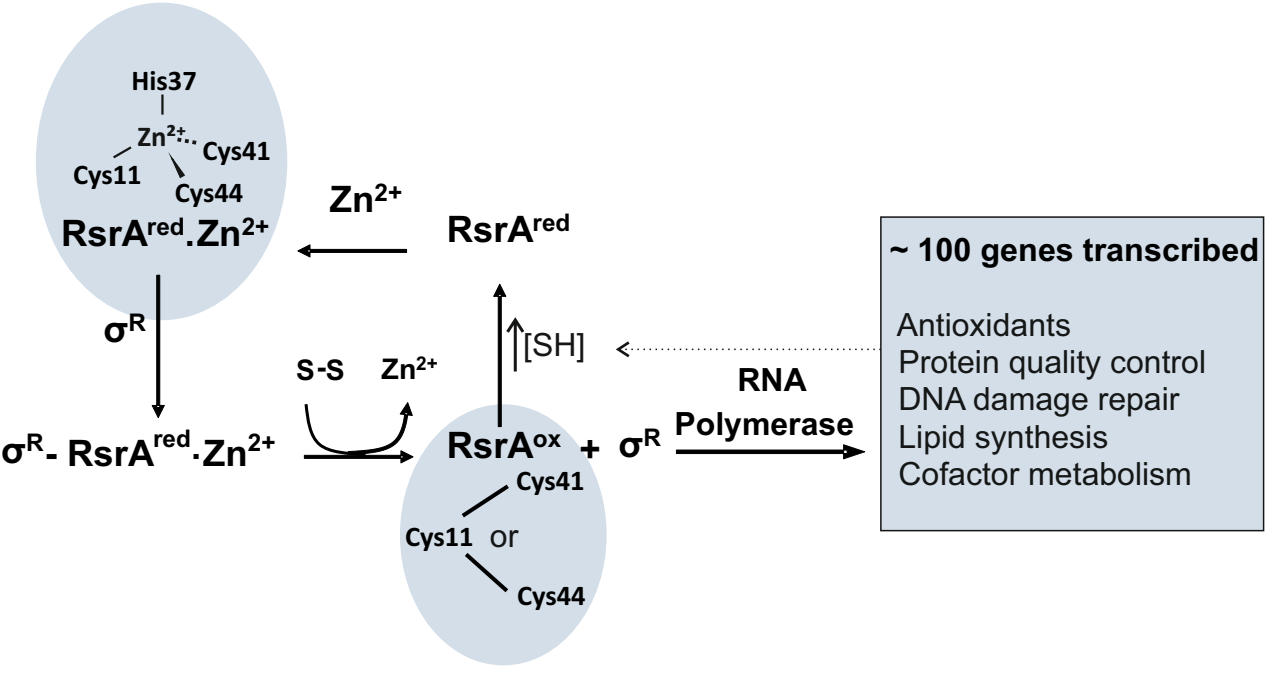
His37
Zn2+
Cys11
Cys41
Cys44
RsrAred.Zn2+
Zn2+
RsrAred
σR
[SH]
S-S
Zn2+
RNA
Polymerase
σR- RsrAred.Zn2+
RsrAox
+
σR
Cys41
Cys11
or
Cys44
~ 100 genes transcribed
Antioxidants
Protein quality control
DNA damage repair
Lipid synthesis
Cofactor metabolism

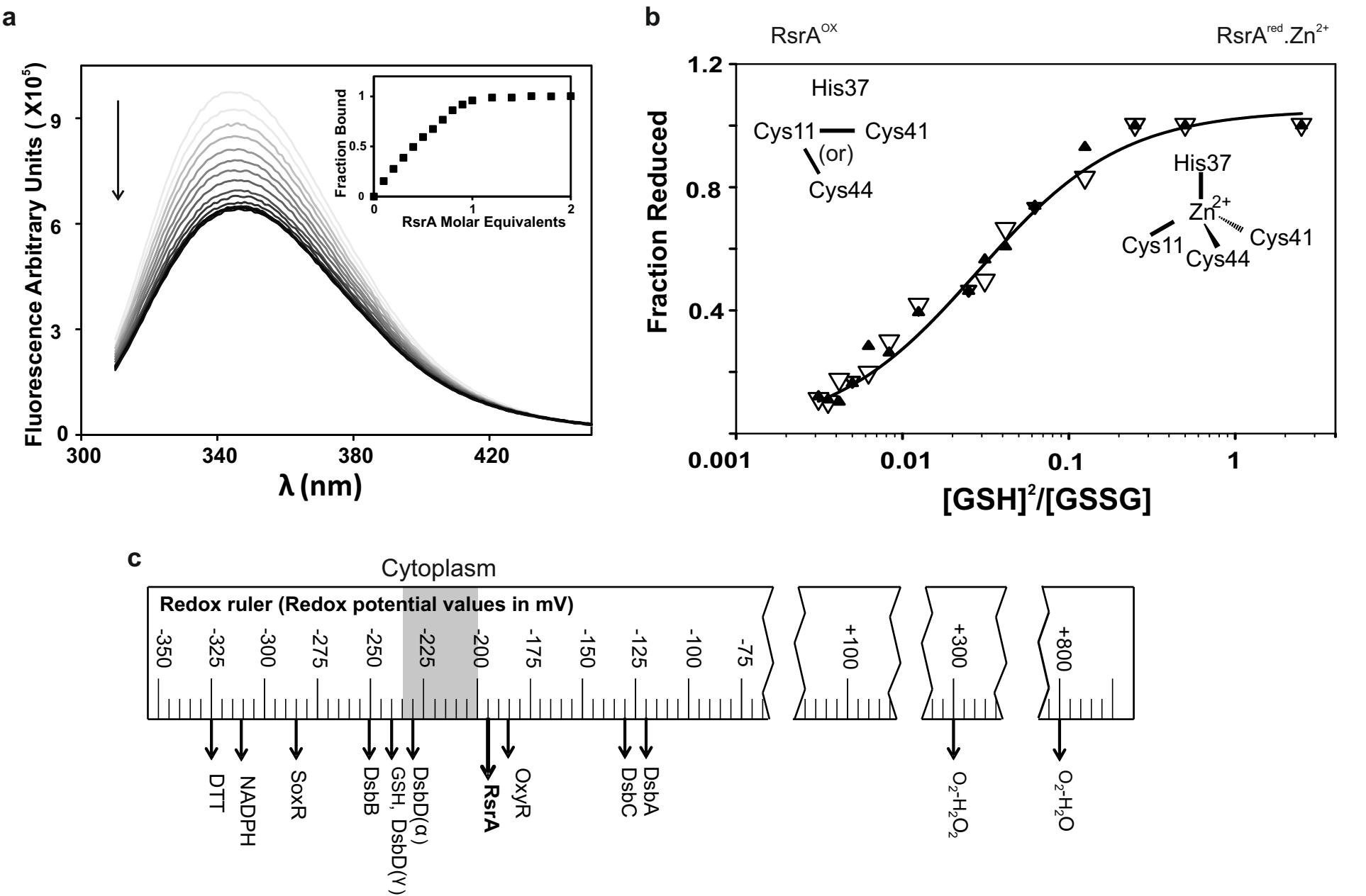
a
Fluorescence Arbitrary Units (X10^5)
λ (nm)
Fraction Bound
RsrA Molar Equivalents
b
RsrA^OX
RsrA^red.Zn^2+
Fraction Reduced
His37
Cys11
Cys41
(or)
Cys44
Zn^2+
[GSH]^2/[GSSG]
c
Cytoplasm
Redox ruler (Redox potential values in mV)
DTT
NADPH
SoxR
DsbB
GSH, DsbD(γ)
DsbD(α)
RsrA
OxyR
DsbC
DsbA
O2-H2O2
O2-H2O

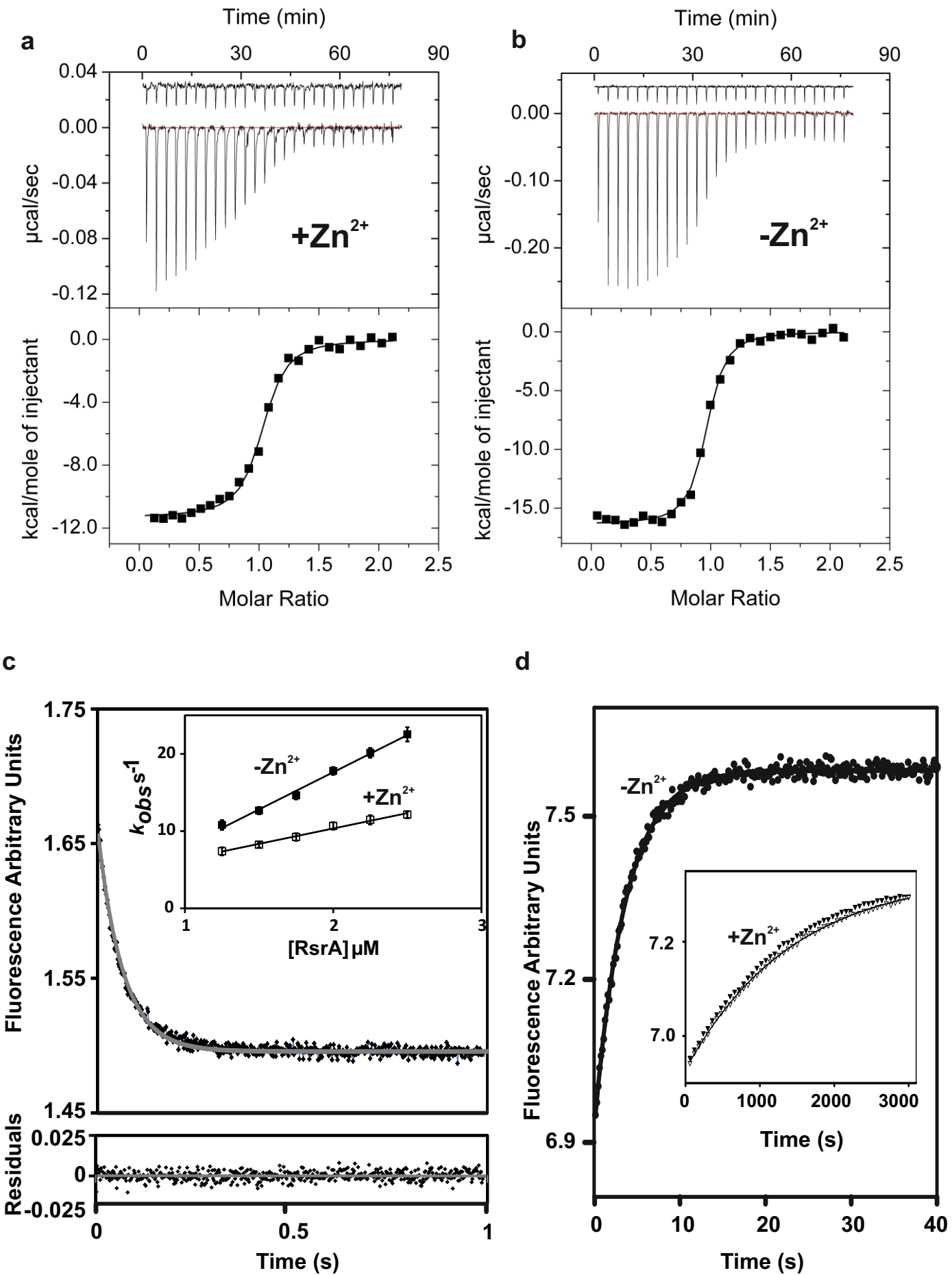
a
Time (min)
0
30
60
90
0.04
0.00
-0.04
-0.08
-0.12
µcal/sec
+Zn2+
0.0
-4.0
-8.0
-12.0
kcal/mole of injectant
0.0
0.5
1.0
1.5
2.0
2.5
Molar Ratio
b
Time (min)
0
30
60
90
0.00
-0.10
-0.20
µcal/sec
-Zn2+
0.0
-5.0
-10.0
-15.0
kcal/mole of injectant
0.0
0.5
1.0
1.5
2.0
2.5
Molar Ratio
c
1.75
1.65
1.55
1.45
Fluorescence Arbitrary Units
kobs s-1
20
10
0
-Zn2+
+Zn2+
1
2
3
[RsrA] µM
0.025
0
-0.025
Residuals
0
0.5
1
Time (s)
d
-Zn2+
7.5
7.2
6.9
Fluorescence Arbitrary Units
+Zn2+
7.2
7.0
0
1000
2000
3000
Time (s)
0
10
20
30
40
Time (s)

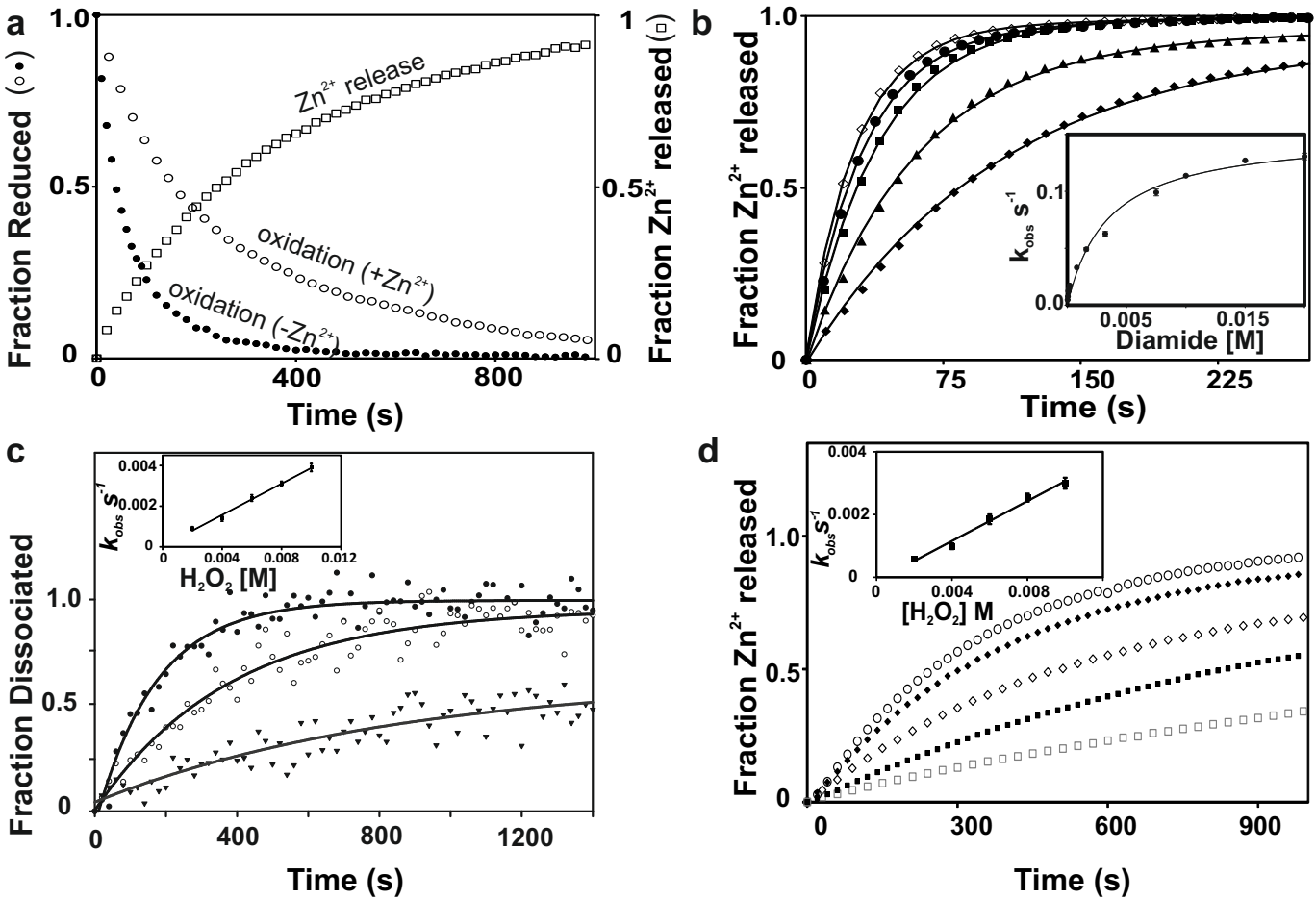
a
Fraction Reduced (•)
Fraction Zn2+ released (□)
Zn2+ release
oxidation (+Zn2+)
oxidation (-Zn2+)
Time (s)
b
Fraction Zn2+ released
kobs s-1
Diamide [M]
Time (s)
c
Fraction Dissociated
kobs s-1
H2O2 [M]
Time (s)
d
Fraction Zn2+ released
kobs s-1
[H2O2] M
Time (s)

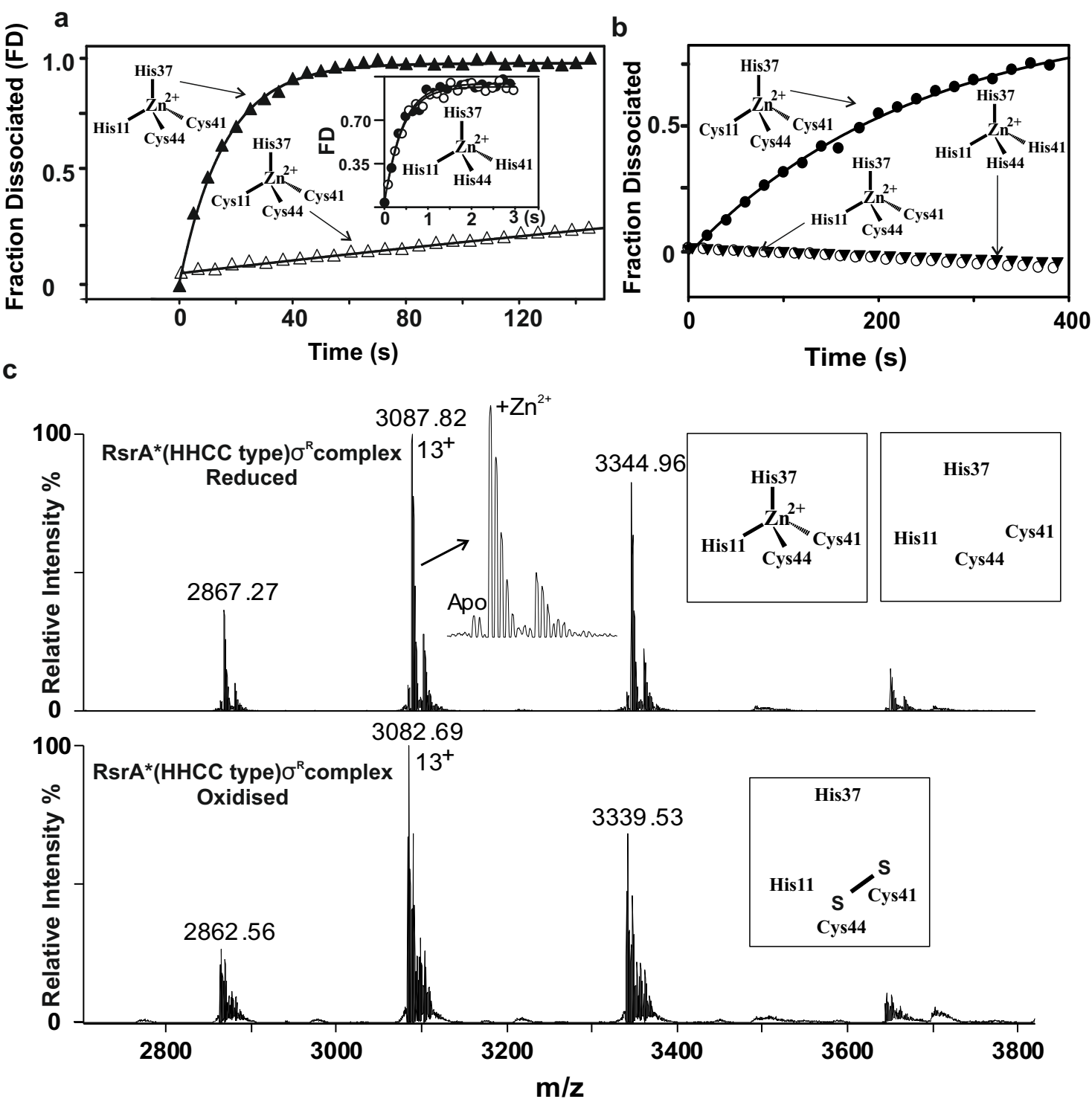
a
Fraction Dissociated (FD)
1.0
0.5
0
0
40
80
120
Time (s)
His37
Zn2+
His11
Cys41
Cys44
Cys11
FD
0.70
0.35
0
1
2
3 (s)
His41
b
Fraction Dissociated
0.5
0
200
400
c
RsrA*(HHCC type)σR complex
Reduced
3087.82
13+
+Zn2+
3344.96
2867.27
Apo
Relative Intensity %
100
0
RsrA*(HHCC type)σR complex
Oxidised
3082.69
13+
3339.53
2862.56
2800
3000
3200
3400
3600
3800
m/z

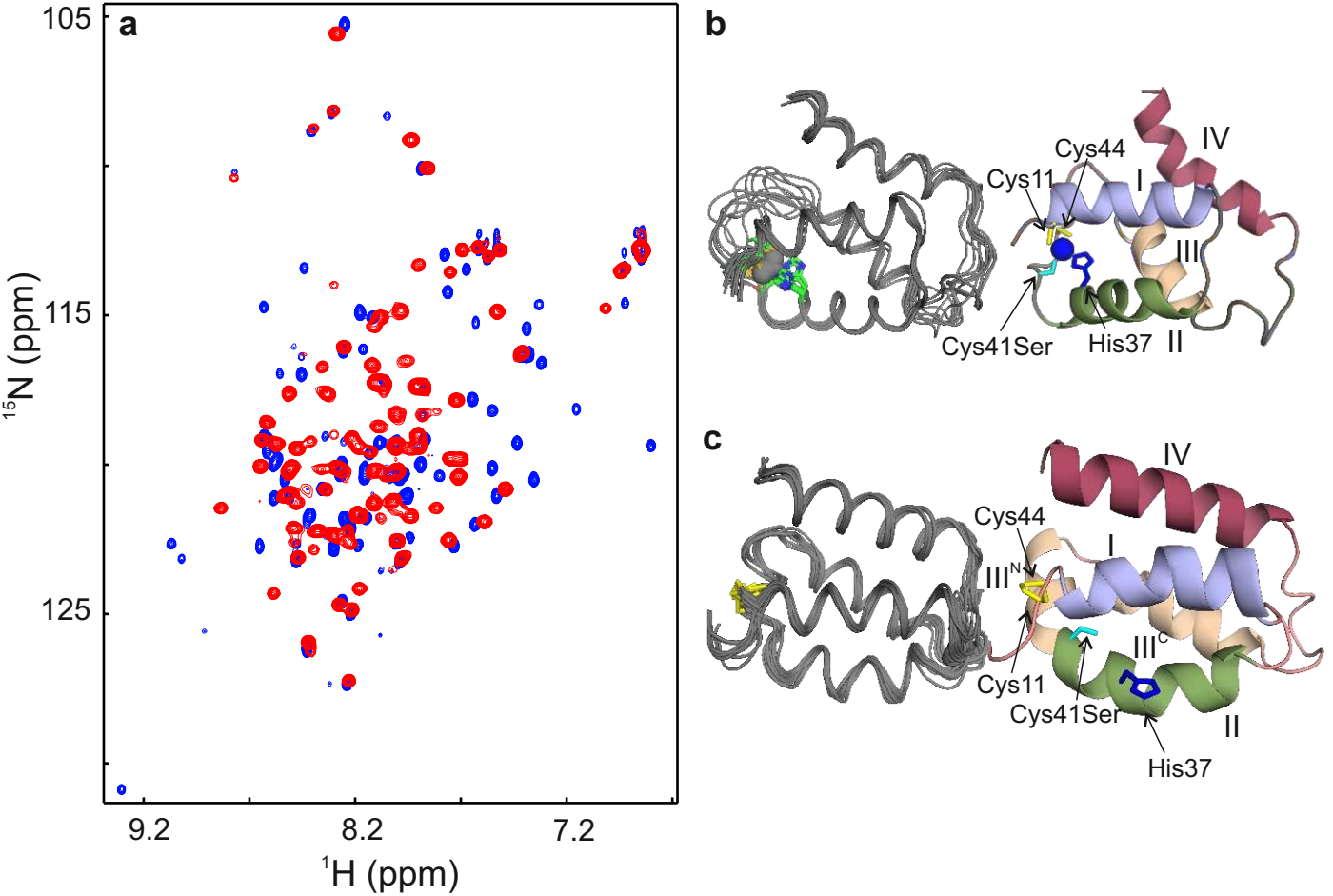
a
105
115
125
^{15}N (ppm)
9.2
8.2
7.2
^{1}H (ppm)
b
Cys44
IV
Cys11
I
III
Cys41Ser
His37
II
c
IV
Cys44
I
III^{N}
III^{C}
Cys11
Cys41Ser
II
His37

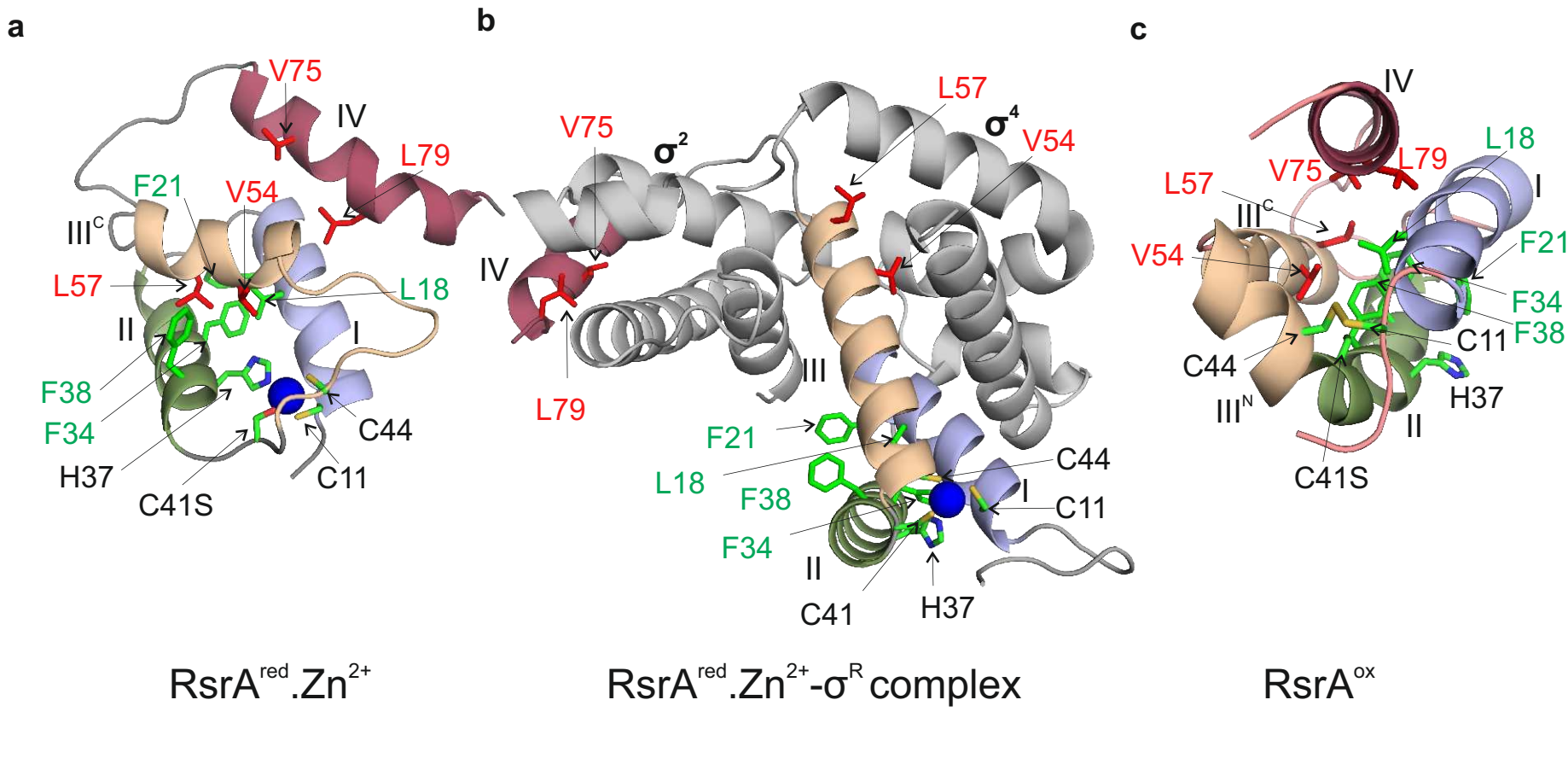
a
V75
IV
L79
F21
V54
III^C
L57
L18
II
I
F38
F34
H37
C44
C11
C41S
b
V75
σ²
L57
σ⁴
V54
IV
L79
III
F21
L18
F38
F34
C44
I
C11
II
C41
H37
c
IV
L18
V75
L79
L57
I
III^C
F21
V54
F34
F38
C11
C44
H37
III^N
II
C41S
RsrA^red.Zn²⁺
RsrA^red.Zn²⁺-σ^R complex
RsrA^ox

d

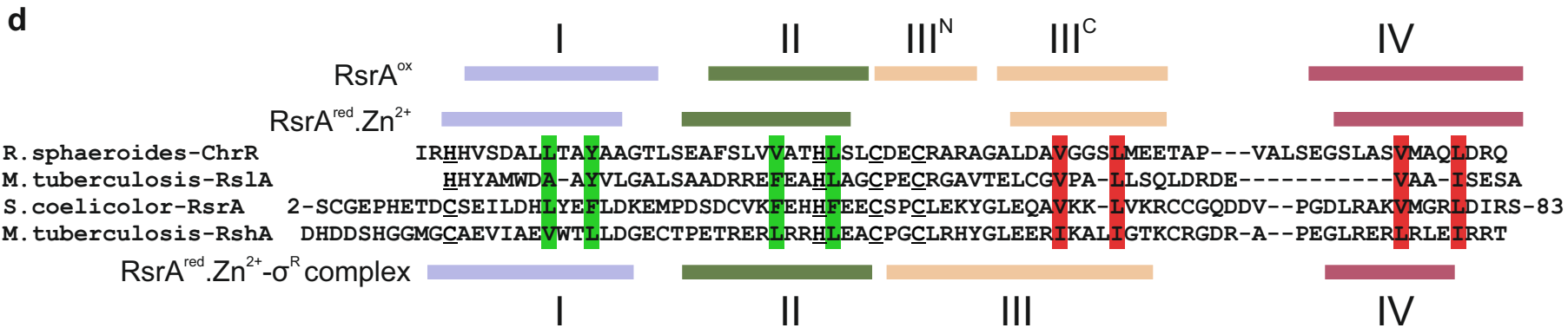
I
II
III^N
III^C
IV
RsrA^ox
RsrA^red.Zn²⁺
R.sphaeroides-ChrR IRHHVSDALLTAYAAGTLSEAFSLVVATHLSLCDECRARAGALDAVGGSLMEETAP---VALSEGSLASVMAQLDRQ
M.tuberculosis-RslA HHYAMWDA-AYVLGALSAADRREFEAHLAGCPECRGAVTELCGVPA-LLSQLDRDE----------VAA-LSESA
S.coelicolor-RsrA 2-SCGEPHETDCSEILDHLYEFLDKEMPDSDCVKFEHHFEECSPCLEKYGLEQAVKK-LVKRCCGQDDV--PGDLRAKVMGRLDIRS-83
M.tuberculosis-RshA DHDDSHGGMGCAEVIAEVWTLLDGECTPETRERLRRHLEACPGCLRHYGLEERIKALIGTKCRGDR-A--PEGLRERLRLEIRRT
RsrA^red.Zn²⁺-σ^R complex
I
II
III
IV

Table 1: NMR and refinement statistics for the structures of $RsrA^{ox}$ and $RsrA^{red}.Zn^{2+}$

	$RsrA^{ox}$	$RsrA^{red}$-Zn^{2+}
NMR distance and dihedral constraints		
Distance constraints		
Total NOE	1532	1033
Intra-residue	749	577
Inter-residue	660	422
Sequential ($\|i-j\|=1$)	333	227
Medium-range ($1<\|i-j\|<4$)	218	108
Long-range ($\|i-j\|>5$)	109	87
Hydrogen bonds	0	0
RDC-based restraints	40	29
Total dihedral angle restraints		
ϕ/ψ	100	104
Structure statistics		
Violations		
Distance constraints > 0.5 Å	0	0
Dihedral angle constraints > 5˚	0	0
Max. dihedral angle violation (º)	4.7	4.6
Max. distance constraint violation (Å)	0.44	0.46
Deviations from idealized geometry (mean and s.d.)		
Bond lengths (Å)	0.005+/-0.0001	0.004+/-0.00007
Bond angles (º)	0.63+/-0.01	0.49+/- 0.01
Average pairwise r.m.s. deviation[b] (Å)		
Heavy	0.84 +/- 0.11	0.82+/- 0.10
Backbone	0.34 +/- 0.07	0.40+/- 0.14
Ramachandran statistics		
Residues in most favoured regions/additional	93.5%	97.7%
Residues in generously allowed regions	5.3%	2.1%
Residues in disallowed regions	1.0% [a]	0

[a] None were well-defined residues. [b] Averaged over secondary structure of 10 lowest energy structures

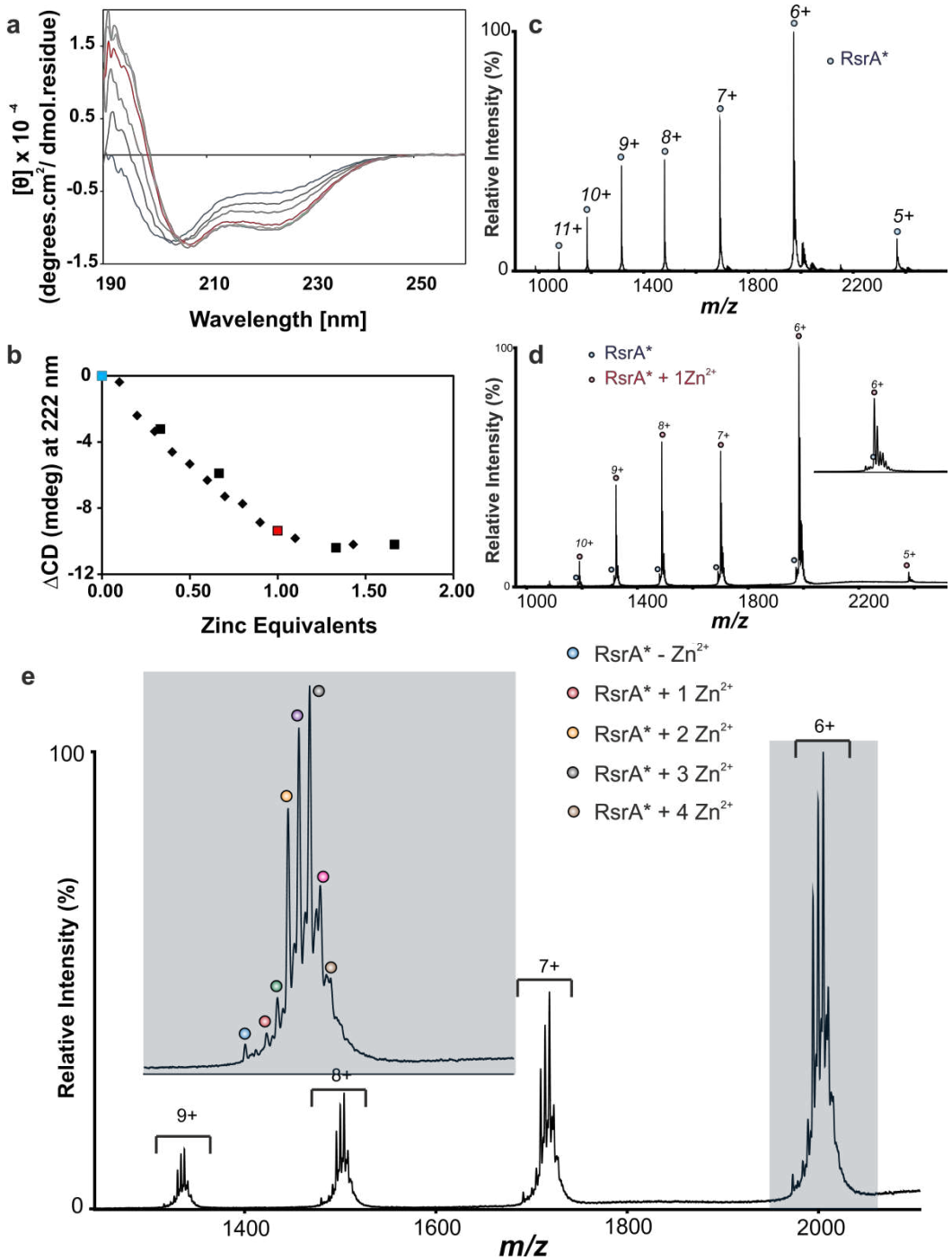

Supplementary Figure 1. Zinc binding to RsrA. ***a***, Far-UV CD spectra of RsrA* incubated with increasing concentrations of zinc (in 10 mM Tris pH 7.5, at 20˚C) starting from apo-protein (*blue spectrum*). Wild type RsrA yielded poor CD spectra and so zinc titrations were performed with RsrA*. The protein becomes more helical as the amount of zinc increases but saturates at one equivalent of zinc (*red spectrum*). ***b***, Figure shows variation of RsrA* mdeg at 222 nm starting from apo-RsrA* (*blue square*, equivalent to blue spectrum in *a*) with increasing zinc concentration. *Red square* is equivalent to the red spectrum in *a*. ***c***, Native-state ESI-MS spectrum of apo-RsrA* (same sample used in CD experiment, blue point in *a*). ***d***, Native-state ESI-MS spectrum of RsrA* incubated with 1 equivalent of zinc (same sample used in CD experiment, red point in *a*). Protein was buffer exchanged into 20 mM ammonium acetate before data collection (theoretical/observed masses for apo- and single zinc bound to RsrA* are 11834/11832.82 ± 0.57 and 11897/11896.75 ± 1.02, respectively). ***e***, Stoichiometry of zinc binding to wild type RsrA. Figure shows the high resolution native-state ESI-MS spectrum of RsrA incubated with excess zinc. 10 µM RsrA was dissolved in 50 mM Tris HCl pH 7.5, 100 mM NaCl, 0.1 mM $ZnCl_2$ and 10 mM DTT. Samples were buffer exchanged into 20 mM ammonium acetate before measurements were made. Spectrum shows up to 3 Zn^{2+} ions bind to RsrA. Theoretical and observed masses for apo, $1Zn^{2+}$, $2Zn^{2+}$ and $3Zn^{2+}$ bound samples were 11962.3/11957.08 ± 4.90 Da, 12025.3/12022.72 ± 6.21 Da, 12088.3/12087.36 ± 5.36 Da and 12151.3/12154.20 ± 4.46 Da respectively. Similar data were obtained for RsrA*, where all non-essential cysteines (Cys3, Cys31, Cys61 and Cys62) were mutated to alanine, indicating that non-stoichiometric zinc binding is not associated with cysteine residues outside of the ZAS sequence motif.

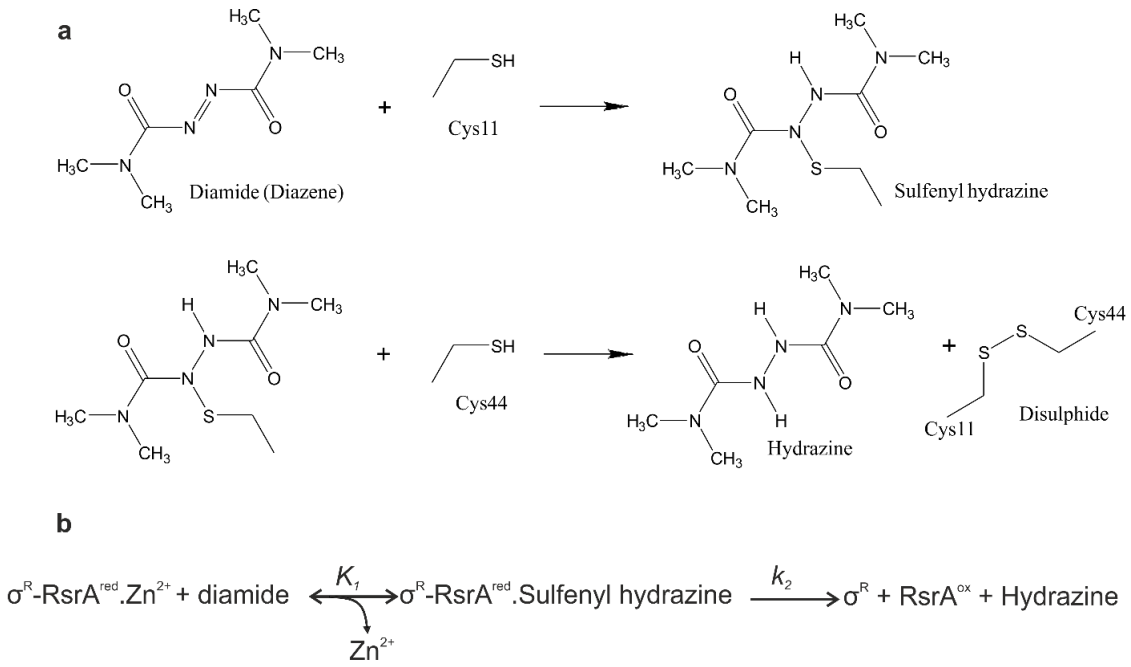

Supplementary Figure 2. Diamide oxidation kinetics. ***a*,** Schematic showing the chemical conversion of diamide from the diazene to hydrazine forms during the oxidation of RsrA. Also shown is the sulfenyl hydrazine intermediate. Spectroscopic measurement of diamide reduction by RsrA exploited the absorption of diamide at 320nm. The product hydrazine does not absorb at this wavelength. ***b*,** Kinetic mechanism for diamide-induced oxidation of $RsrA^{red}.Zn^{2+}$. The mechanism is based on data obtained from diamide reduction kinetics (main text, **Figure 4b**). Values for K_1 and k_2 obtained from the data shown in Figure 4b were 0.7 mM and 0.15 s^{-1}, respectively. ***c***, Kinetics of $RsrA^{red}.Zn^{2+}$ oxidation by diamide are the same as for the $RsrA^{red}.Zn^{2+}$-σ^R complex. Experiments were conducted at 25˚C in 50 mM Tris HCl pH 7.5 buffer containing 100 mM NaCl. Proteins were first reduced with DTT (10 mM) then buffer exchanged to remove the reducing agent. Where indicated, stoichiometric zinc was added. Oxidation of and zinc release from $RsrA^{red}.Zn^{2+}$ on treatment with diamide under second-order conditions (25 μM) was measured spectrophotometrically (see Materials and Methods for further details). The fraction of reduced $RsrA^{red}.Zn^{2+}$ was determined by monitoring the change in diamide absorbance at 320 nm in the presence and absence of stoichiometric zinc (*open and closed circles*, respectively). Zinc release (*open squares*) was monitored at 500 nm using the PAR assay. For clarity, only every 80th data point is shown in these curves. The two methods showed good agreement for the bimolecular rate constant for diamide-induced oxidation of $RsrA^{red}.Zn^{2+}$ (196 ± 12.3 M^{-1} $s^{-1}$and 194 ± 29 M^{-1} s^{-1}, respectively). Oxidation of RsrA was five-fold faster in the absence of zinc (946 ± 24 M^{-1} s^{-1}). These data closely mirror those obtained for RsrA bound to σ^R indicating that complex formation does not influence redox sensing by RsrA.

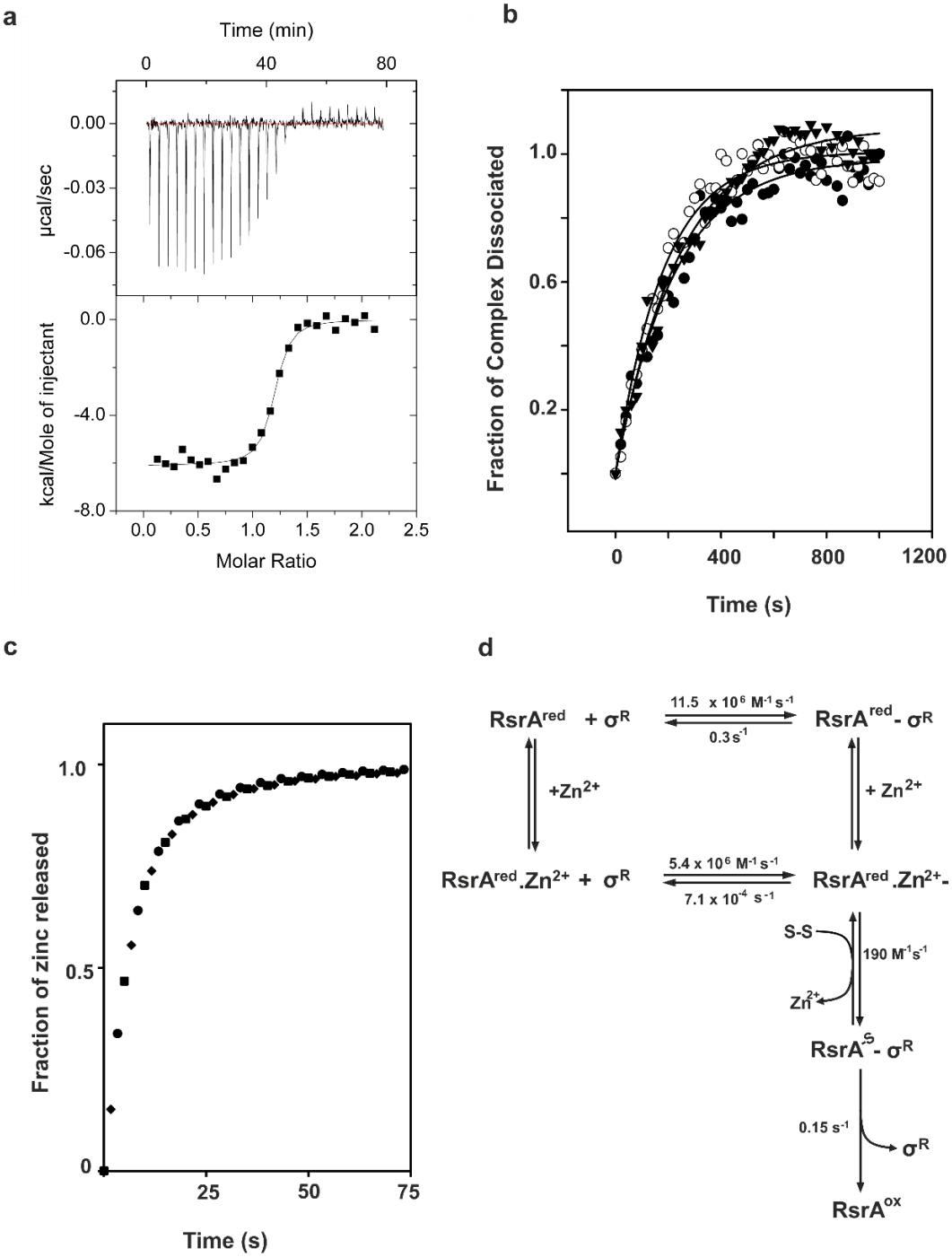

Supplementary Figure 3. Additional Zn^{2+} ions do not affect the rate of RsrA oxidation. ***a***, Competition ITC data for σ^R Trp88Ile Trp119Ile binding $RsrA^{red}.Zn^{2+}$, as described for the wild type complex (main text, **Figure 3a**). Fitted parameters for a single binding site model were N = 1.17 ± 0.09, K_d = 0.173 ± 0.034 nM, ΔH = -20.34 ± 0.91 kcal/mol. ***b***, Tryptophan emission fluorescence spectroscopy was used to determine the kinetics of $RsrA^{red}$-σ^R oxidative dissociation on treatment with 10 mM H_2O_2 and increasing zinc stoichiometry. Oxidation induced dissociation of the $RsrA^{red}$-σ^R complex was the same regardless of whether 1 (*open circles*), 2 (*closed triangles*) or 3 (*closed circles*) equivalents of zinc, respectively, were added to the protein. ***c***, The rate of Zn^{2+} release from the $RsrA^{red}.Zn^{2+}$-σ^R complex on treatment with 15 mM diamide is the same when RsrA is bound with 1 (*diamonds*), 2 (*circles*) or 3 (*squares*) equivalents of zinc, respectively. Hence, increasing zinc stoichiometry does not influence redox sensing by the $RsrA^{red}.Zn^{2+}$-σ^R complex. *d*, Kinetic scheme of RsrA-σ^R interaction. ***d***, Kinetic scheme showing RsrA-σ^R protein-protein interactions and the influence of zinc and oxidant. Rate constants are taken from Figures 4 and 5. The kinetics of $RsrA^{red}.Zn^{2+}$-σ^R oxidation are those for a disulfide-containing oxidant, denoted by S-S in the scheme and mimicked by diamide in our experiments, to form a mixed disulfide ($RsrA^{-S}$), which we infer (Figure 4b). The oxidation process is a two-step reaction involving the slow loss of zinc followed by a fast step involving dissociation of σ^R and formation of the trigger disulfide bond (Cys11-Cys44 or Cys11-Cys41).

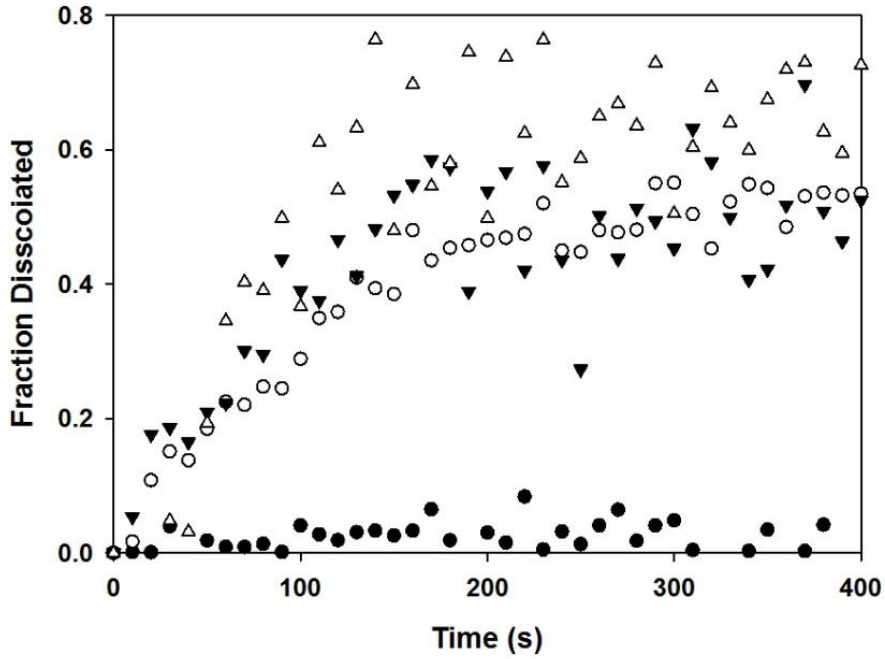

Supplementary Figure 4. H_2O_2-induced dissociation of RsrA histidine mutants confirms the redundancy of the trigger disulfide bond. Comparison of H_2O_2 (10 mM) induced dissociation of RsrA^{*red}.Zn^{2+}-σ^R complex (*open circles*) with RsrA^{*red}.Zn^{2+} Cys11His-σ^R (*closed circles*), RsrA^{*red}.Zn^{2+} Cys41His-σ^R (*closed triangles*) and RsrA^{*red}.Zn^{2+} Cys44His-σ^R (*open triangles*) complexes. The data emphasise the redundancy of the trigger disulfide bond in RsrA in which either Cys41 or Cys44 can form a disulfide with Cys11 to release σ^R.

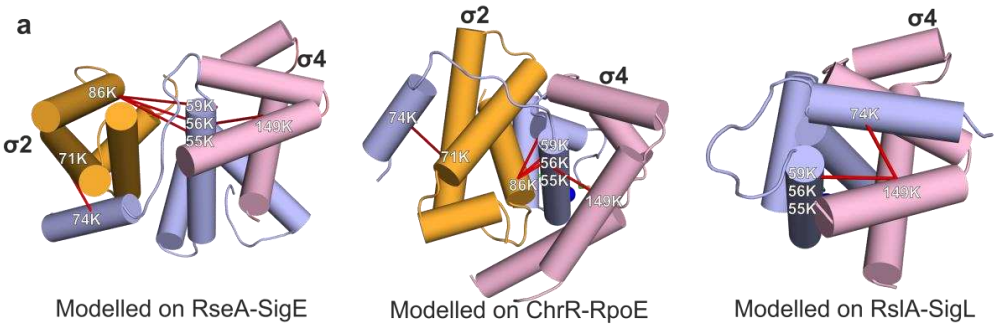

	X-walk distance (Solvent Accessible Surface Distance Å)					
Model	**RseA-σ^E**		**ChrR-RpoE**		**RslA-σ^L**	
Observed Cross links (BS3=✓✓, BS2G=✓)	**Distance**	**Cross link expected**	**Distance**	**Cross link expected**	**Distance**	**Cross link expected**
RsrA56K-σR86K ✓✓	15.6	✓	4.4	✓✓	NK	
RsrA55K-σR86K ✓✓	22.4	×	9.6	✓✓	NK	
RsrA59K-σR86K ✓✓	19.3	×	5.7	✓✓	NK	
RsrA74K-σR71K ✓✓	22.7	×	14.1	✓✓	NK	
RsrA74K-σR86K ✓✓	>50	×	>50	×	NK	
RsrA74K-σR149K ✓✓	>50	×	>50	×	6.2	✓✓
RsrA56K-σR149K ✓	15.8	✓	8.5	✓✓	15.8	✓

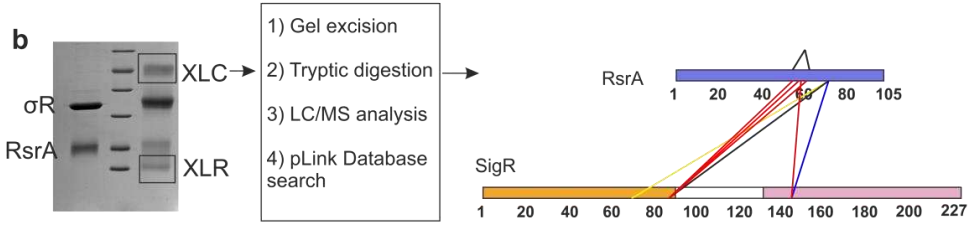

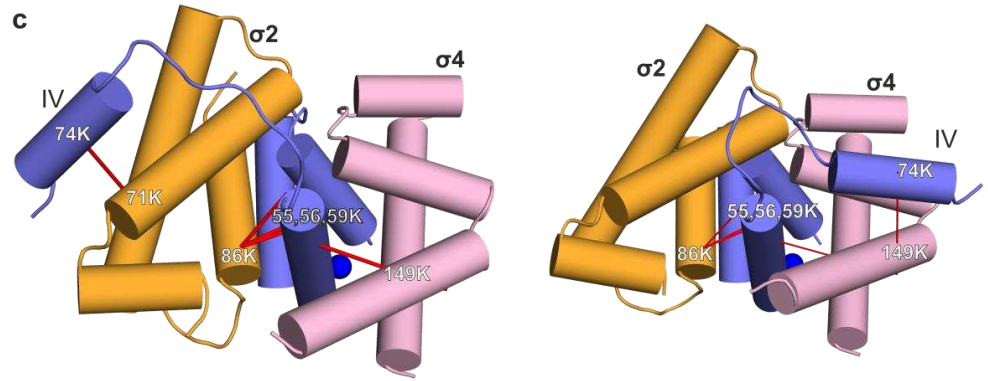

Supplementary Figure 5. Cross-linking based homology model of the RsrA^{red}.Zn^{2+}-σ^R complex. ***a,*** The RsrA^{red}.Zn^{2+}-σ^R complex (RsrA, blue; σ^R σ^2 domain, orange, and σ^4 domain, pink) was modelled on three anti-sigma factor-sigma factor complexes, *E. coli* RseA-σ^E (sequence identity 15.8%, pdb code 1OR7), *R. sphaeroides* ChrR-RpoE/σ^E (sequence identity 11.1%, pdb code 2Q1Z) and *M. tuberculosis* RslA-σ^L (sequence identity 20.6%, pdb code 3HUG). Only ChrR and RslA are ZAS proteins but all three have the so-called ASD fold. The structure of the RslA-σ^L complex only contains half of the sigma factor (σ^4 domain) whereas the other complexes have both σ^2 and σ^4 domains. Red lines indicate the lysine-specific crosslinks observed for the RsrA^{red}.Zn^{2+}-σ^R complex mapped onto each model. The table beneath the structures shows the solvent accessible surface distances for lysines in the RsrA^{red}.Zn^{2+}-σ^R complex predicted for the different models and summarizes the cross-links observed for the different homo-bifunctional cross-linkers used (BS3, bis(sulfosuccinimidyl)suberate, 11.4 Å cross-linking distance; BS2G, bis(sulfosuccinimidyl) 2,2,4,4-glutarate), 7.7 Å cross-linking distance. NK, not known. The cross-links observed in the RsrA^{red}.Zn^{2+}-σ^R complex (*left hand panel*) indicated the complex was most similar to the ChrR-RpoE complex but also had similarities to the RslA-σ^L complex. ***b***, Strategy used to obtain lysine-specific cross-linking data for the RsrA^{red}.Zn^{2+}-σ^R complex. RsrA^{red}.Zn^{2+}-σ^R complex was incubated with a 2 mM mixture of BS^{2}G-d$_0$ and BS^{2}G-d$_4$ in 20 mM Hepes pH 7.5, 50 mM NaCl and 2 mM DTT at room temperature for 30 minutes. Cross-linking was stopped with 100 mM Tris pH 7.5. Samples were run on an SDS-PAGE and protein bands excised and analysed by LC-MS/MS. (Crosslinking with BS3-d$_0$/BS3-d$_4$ was done similarly). Crosslinks to all residues except RsrA K74 are coloured red. Crosslinks to RsrA K74 to σ^R K71 is coloured yellow, RsrA K74 to σ^R K86 is coloured black and RsrA K74 to σ^R K149 is coloured blue. A single unique intramolecular cross-link within RsrA (56K-74K) was observed (XLR in the gel) which agrees with the solution structure of RsrA^{red}.Zn^{2+}. ***c***, Homology model of the RsrA^{red}.Zn^{2+}-σ^R complex showing two possible conformations of helix IV. Model was built based on homology with ChrR-RpoE and RslA-σ^L using Modeller V9.12. 100 models were generated and the lowest energy model shown. RsrA is coloured blue, σ^2 domain of σ^R is coloured orange, σ^4 domain of σ^R is coloured pink. Cylinders denote helices and are coloured as in *a*. Red lines denote the observed crosslinks. RsrA keeps the same fold in both the models except for the orientation of the final helix which could interact with either σ^2 or σ^4.

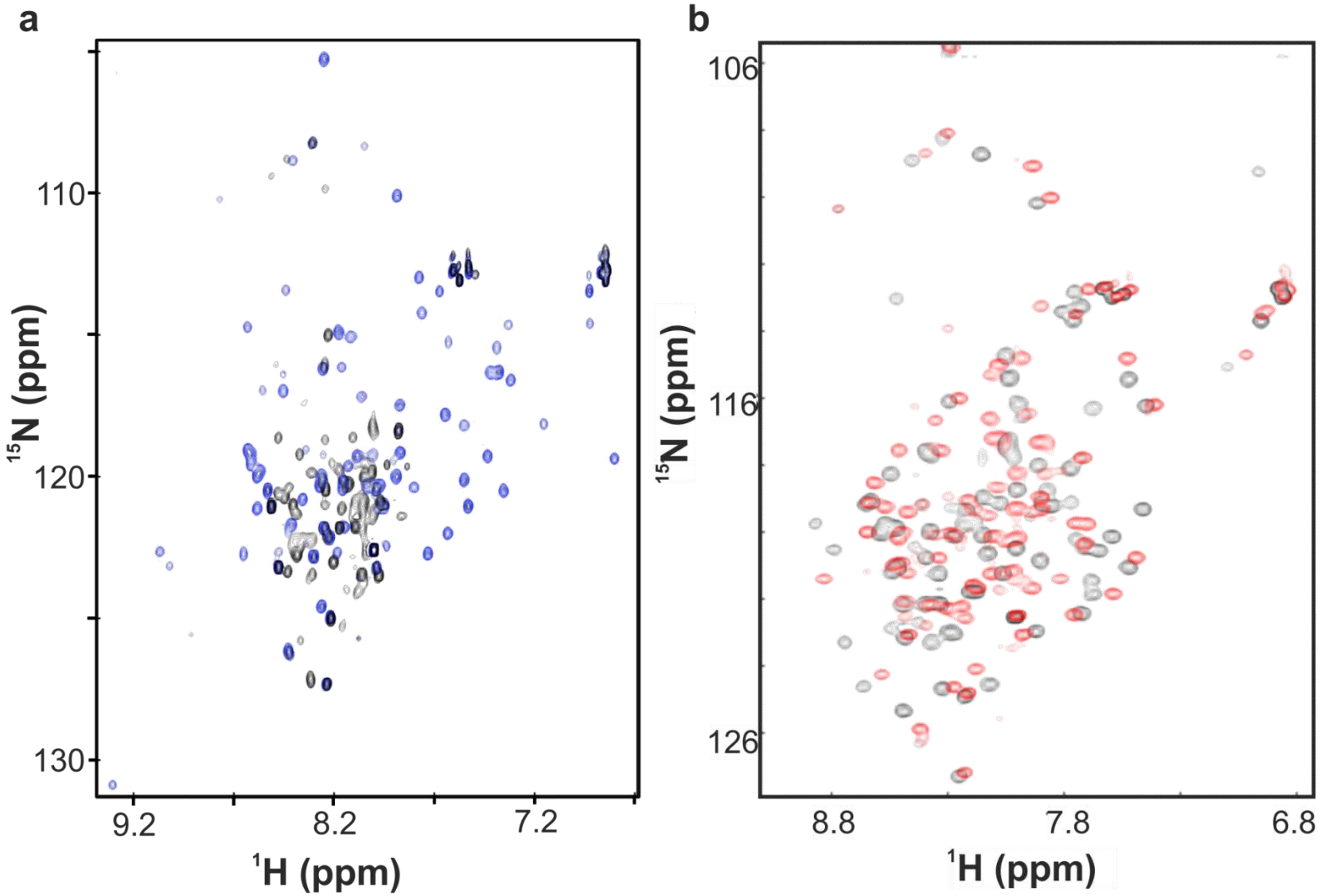

Supplementary Figure 6. ^{1}H-^{15}N HSQC spectra of reduced and oxidized RsrA. ***a***, ^{1}H-^{15}N-HSQC spectrum of RsrA^{*red} Cys41Ser in the absence of zinc (black) and bound to one equivalent of zinc (blue) in 20 mM Tris buffer pH 7.1 containing 5 mM DTT and 2 mM $ZnCl_2$. ***b***, Oxidised RsrA proteins containing either Cys11-Cys41 or Cys11-Cys44 disulfide bonds yield well-dispersed HSQC spectra characteristic of globular, folded proteins. Overlay of HSQC spectra of oxidized RsrA* Cys44Ser containing the Cys11-Cys41 disulfide bond (*black peaks*) and RsrA* Cys41Ser containing the Cys11-Cys44 disulfide bond (*red peaks*).

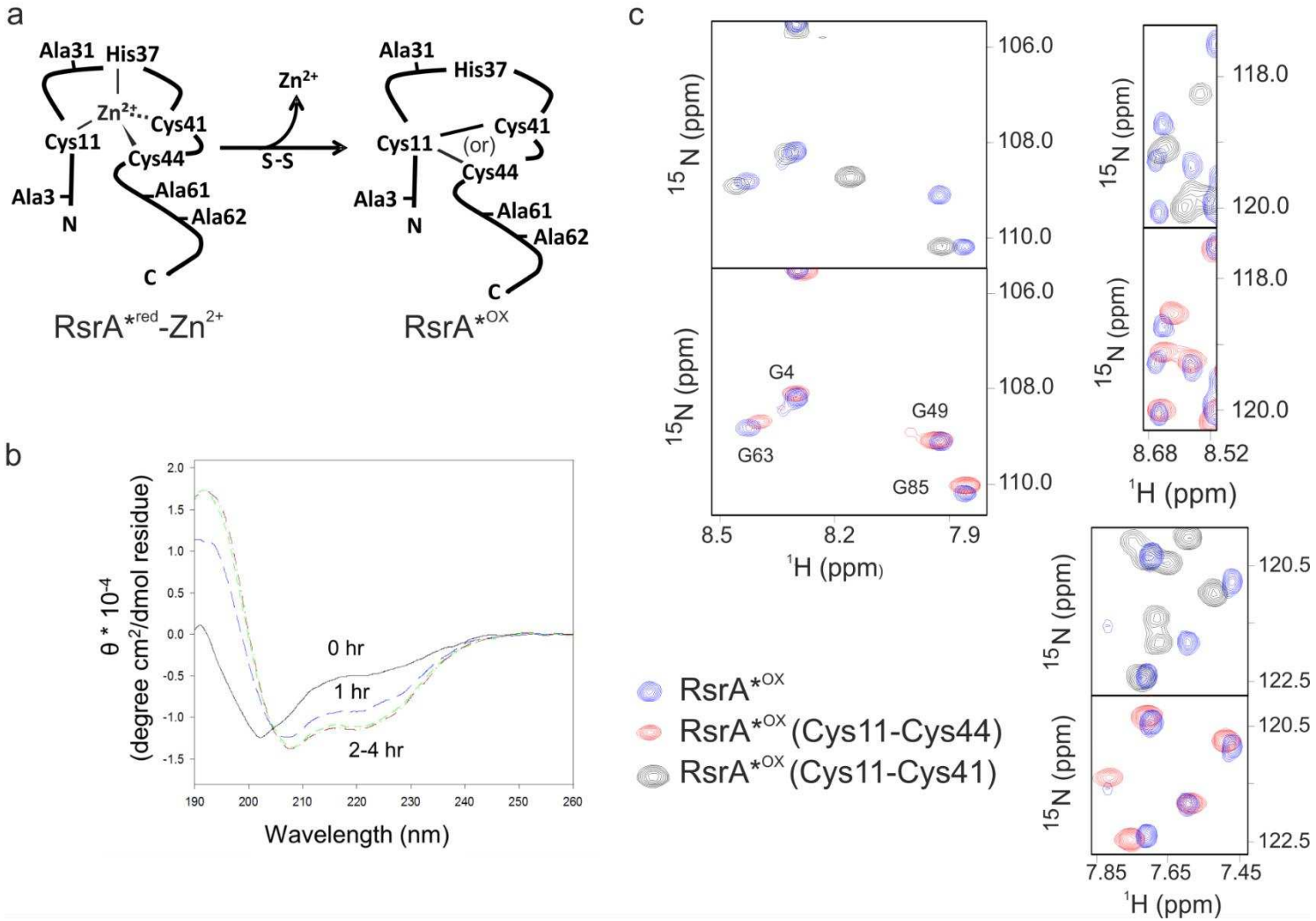

Supplementary Figure 7. Identification of the most stable trigger disulfide bond in RsrA^{ox}. ***a***, Schematic of RsrA showing the location of cysteine residues mutated to alanine in RsrA*, the identity of the zinc ligands and the trigger disulfide bond that forms in response to oxidation and which results in the loss of zinc. Previous studies have shown that the trigger disulfide is degenerate and forms between either Cys11 and Cys41 or Cys11 and Cys44. ***b***, Time-dependent changes in far UV-CD spectra (0.16 mg/ml) during formation of the RsrA* Cys11-Cys44 disulfide bond in RsrA* C41S as a result of air oxidation in 20 mM Tris pH 7.1, 25°C are similar to those previously reported for wild-type RsrA [25]. ***c***, Overlay of ^{1}H-^{15}N-HSQC spectra of air-oxidized RsrA* (*blue peaks*), from which zinc had been removed, with ^{1}H-^{15}N-HSQC spectra of RsrA*^{ox} containing either the Cys11-Cys41 disulfide bond (*black peaks*) or the Cys11-Cys44 disulfide bond (*red peaks*). In each of the pure disulfided species of RsrA the third cysteine was mutated to serine to block mixed disulfide bond formation. The figure shows a comparison of three chemical shift regions demonstrating the overall similarity of the spectra of RsrA*^{ox} with RsrA*^{ox} containing the Cys11-Cys44 disulfide bond (lower panels in the three spectral regions shown) rather than the Cys11-Cys41 disulfide bond. Assignments for glycine residues in RsrA*^{ox} Cys11-Cys44 are shown.

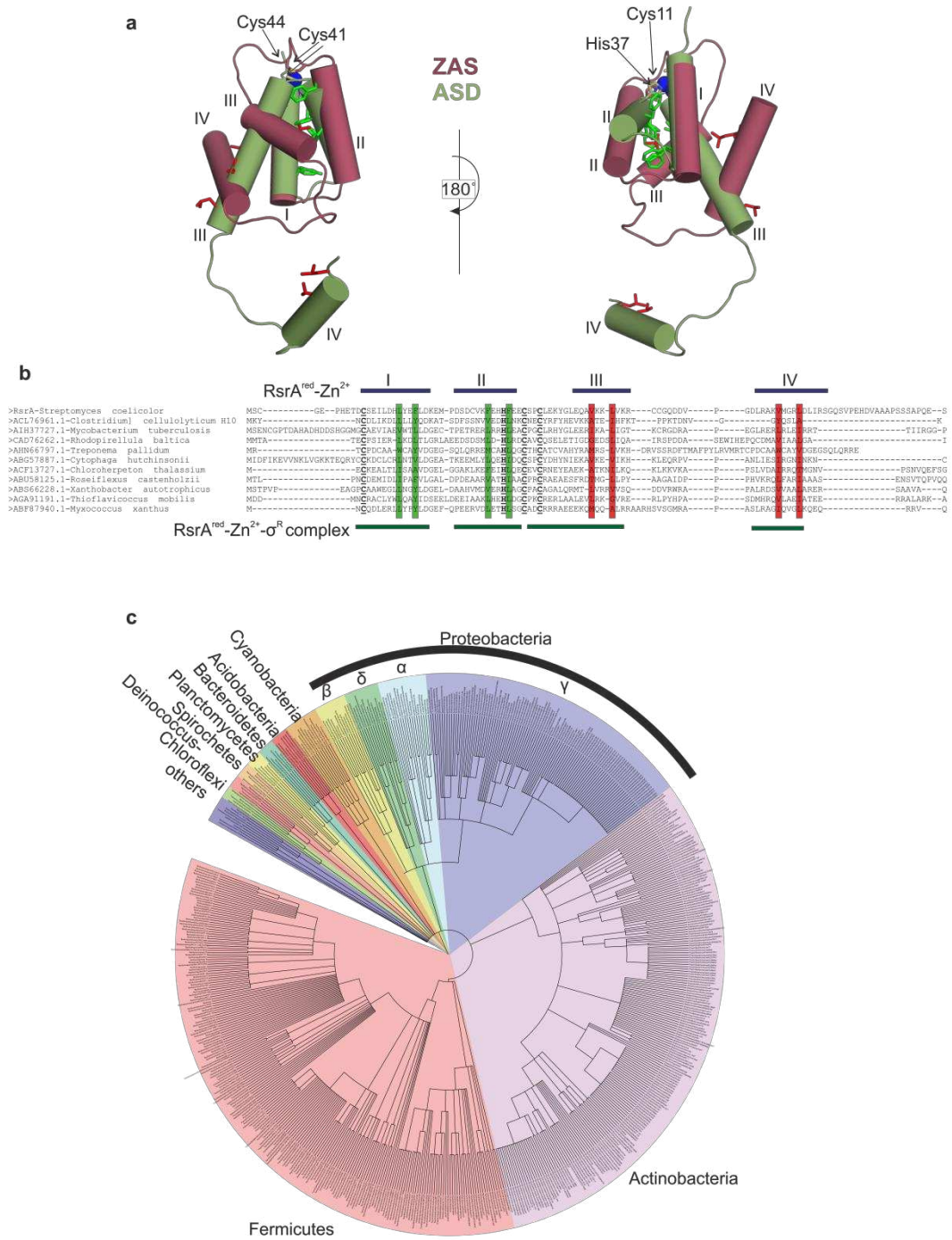

Supplementary Figure 8. Comparison of the ZAS and ASD folds. ***a***, Structural alignment of RsrA^{red}-Zn^{2+}(ZAS fold coloured *red*) and RsrA^{red}-Zn^{2+} in complex with σ^R (ASD fold coloured *green*). Helices are numbered from I to IV. Zinc is shown as a *blue sphere*, zinc ligands are shown as sticks and coloured based on atom type. Hydrophobic residues that form RsrA's core in both RsrA^{red}-Zn^{2+} and the RsrA^{red}-Zn^{2+}-σ^R complex are shown as *green sticks*. Hydrophobic residues that form RsrA's core in RsrA^{red}-Zn^{2+} but also form interactions with the sigma factor in the RsrA^{red}-Zn^{2+}-σ^R complex are shown as *red sticks*. The figure highlights how the ASD and ZAS folds represent different structural states of the same anti-sigma factor. ***b***, Structure-based sequence alignment of distantly related ZAS proteins from different phyla. *Streptomyces* and *Mycobacterium* belong to actinobacteria, *Clostridium* belongs to Firmicutes, *Rhodopirellula* under Planctomycetes, *Treponema* under Spirochaetes, *Cytophaga* under Bacteroidetes, *Chloroherpeto* under Chlorobi, *Roseiflexus* under Chloroflexi, *Zantobacter, thioflavicoccus and Myxococcus* under Proteobacteria. Helix limits of RsrA^{red}-Zn^{2+} and RsrA^{red}Zn^{2+}-σ^R complex are shown by *blue* and *green* horizontal bars, respectively. Hydrophobic residues are coloured as in *a*. Conserved hydrophobic residues in helices I and II (*green*) are involved primarily in stabilizing both the ZAS and ASD folds. In contrast, conserved hydrophobic residues in helices III and IV (*red*) have a dual role, stabilizing the ZAS fold in the absence of sigma factor and the protein-protein interaction with sigma factor. ***c***, Abundance of ZAS-ECF complexes in bacteria. The figure shows all organisms that have a ZAS domain close to an ECF. Searching for proteins similar to RsrA or ChrR with a zinc motif (C/H-x(23-26)-H-x(3)-C-x(2)-C) that lie less than 300 bases away from an ECF-σ homolog showed that more than 1100 genomes have ECF-ZAS pairs. Different sector colours denote different phyla.

Residues / Protein	3	11	31	41	44	61	62	K_d (nM)	ΔH (kcal/mol)	ΔS (cal/mol/deg)
RsrA (+) Wild type	C	C	C	C	C	C	C	0.78 ± 0.034	-23.05 ± 1.10	-38.70 ± 3.10
RsrA (-) Wild type	C	C	C	C	C	C	C	79.3 ± 4.2	-16.26 ± 0.13	-20.3 ± 4.34
RsrA* (+)	A	C	A	C	C	A	A	0.23 ± 0.031	-19.64 ± 2.14	-30.06 ± 4.70
RsrA* (-)	A	C	A	C	C	A	A	183 ± 7.1	-11.51 ± 0.24	-5.61± 0.71
RsrA* C41S (+)	A	C	A	S	C	A	A	557 ± 45.8	-14.81 ± 0.33	-19.50 ± 0.87
RsrA* C44S (+)	A	C	A	C	S	A	A	ND	ND	ND
RsrA* C11S (+)	A	S	A	C	C	A	A	79 ± 19	-19.22 ± 0.91	-29.87 ± 3.33
RsrA* C41S C44S (+)	A	C	A	S	S	A	A	297 ± 44.5	-18.77 ± 1.23	-31.10 ± 3.50
RsrA* C11S C44S (+)	A	S	A	C	S	A	A	185 ± 22.8	-15.27 ± 0.25	-18.60 ± 0.60
RsrA* C11S C41S (+)	A	S	A	S	C	A	A	240 ± 4.2	-17.12 ± 0.54	-25.45 ± 2.33
RsrA* C11H C41H C44H (+)	A	H	A	H	H	A	A	305 ± 2	-15.76 ± 0.68	-22.60 ± 0.70
RsrA V54A L57A (+)	C	C	C	C	C	C	C	105 ± 10.8	-23.80 ± 1.48	-46.2 ± 3.03
RsrA V75A L79A (+)	C	C	C	C	C	C	C	82.1 ± 2.24	-15.5 ± 0.84	-18.5 ± 2.16

Supplementary Table 1: Affinity of wild type and mutant RsrA proteins for σ^R in the presence (+) or absence (-) of Zn^{2+} determined by ITC. Table shows the identity of residues at each of the six cysteines in RsrA. Data for RsrA mutants of σ^R-contacting hydrophobic residues (final two rows) are also shown. RsrA* denotes RsrA in which all non-zinc ligating cysteines were mutated to alanine. See text for details. *ND*, not detected. Conditions for all experiments were 50 mM Tris pH 7.5 buffer containing 100 mM NaCl and 2 mM DTT, 35°C. No heats of binding could be detected at 25°C. Mean values are shown in the table along with standard deviations from three independent measurements.

25°C	k_{on} **($M^{-1}s^{-1}$)**	k_{off} **(s^{-1})**	K_d **(nM) from kinetics**	K_d **(nM) from ITC**
+ Zn^{2+}	5.4 ± 0.2 x 10^6	7.1 x 10^{-4} ± 2 x 10^{-5}	0.13	ND
- Zn^{2+}	11.49 ±1.69 x 10^6	0.286 ± 0.051	24.9	ND
35°C				
+ Zn^{2+}	8.9 ± 1.4 x 10^6	0.0024 ± 0.0004	0.27	0.78 ± 0.034
- Zn^{2+}	17.3 ±1.3 x 10^6	1.08 ± 0.01	62.4	79.3 ± 4.2

Supplementary Table 2: Association (k_{on}) and dissociation (k_{off}) rate constants for the RsrA-σ^R complex in the presence or absence of Zn^{2+} at 25°C and 35°C. Mean values are shown along with standard deviations from three independent measurements. The kinetically-derived K_ds (k_{off}/k_{on}) at 35°C show reasonable agreement with those obtained by ITC, presented alongside for comparison. The affinity of the complex at 25°C in the presence of zinc is ~2-fold higher compared to 35°C. *ND*, not determined. Conditions for all experiments were 50 mM Tris pH 7.5 buffer containing 100 mM NaCl and 2 mM DTT.

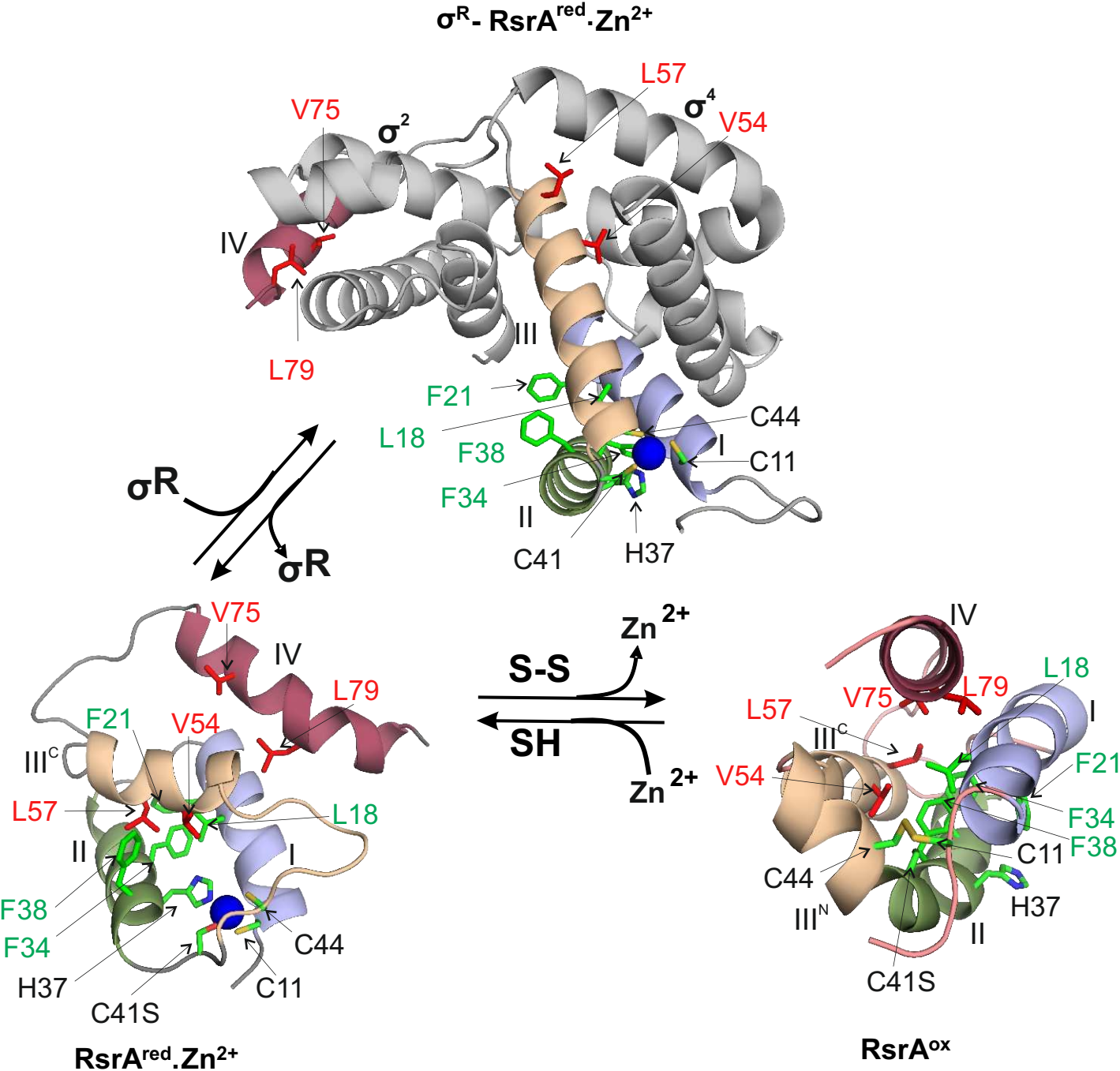
σR- RsrAred·Zn2+
L57
V75
σ2
σ4
V54
IV
III
L79
F21
L18
C44
F38
I
C11
F34
II
C41
H37
σR
σR
V75
IV
L79
F21
V54
IIIC
L57
L18
II
I
F38
F34
C44
H37
C11
C41S
Zn 2+
S-S
SH
Zn 2+
IV
L18
L79
V75
L57
I
IIIC
V54
F21
F34
C11
F38
C44
IIIN
H37
II
C41S
RsrAred.Zn2+
RsrAox